

Characteristics of mesoscale convection over northwestern Mexico, the Gulf of California, and Baja California Peninsula

Luis M. Farfán¹  | Bradford S. Barrett²  | G. B. Raga³  | Julián J. Delgado⁴ 

¹Unidad La Paz, Centro de Investigación Científica y de Educación Superior de Ensenada, La Paz, Mexico

²Oceanography Department, U.S. Naval Academy, Annapolis, Maryland

³Centro de Ciencias de la Atmósfera, Universidad Nacional Autónoma de México, Ciudad de México, Mexico

⁴Departamento de Cómputo, Centro de Investigación Científica y de Educación Superior de Ensenada, Ensenada, Mexico

Correspondence

Luis M. Farfán, Centro de Investigación Científica y de Educación Superior de Ensenada (CICESE), La Paz, Baja California Sur 23050, México.
Email: farfan@cicese.edu.mx

Funding information

Centro de Investigación Científica y de Educación Superior de Ensenada, Baja California, Grant/Award Number: 691-103; Bureau of Educational and Cultural Affairs, Fulbright Scholar Program; Universidad Nacional Autónoma de México, Grant/Award Numbers: IA104416, IA101418

Abstract

Mesoscale convective systems (MCSs) are frequent, but understudied, components of the warm season climatology in northwestern Mexico. This study provides an update of previous research on convective development and examines MCS life cycle, structure, and motion from July through September. It focuses on a region south of the North American monsoon core and, from 2009 to 2018 satellite observations, on patterns of cloud tops higher than 10 km above sea level. The diurnal cycle of convection shows cells initiating in the early afternoon over the Sierra Madre Occidental mountains and becoming better organized over the next few hours. These features typically move westward, grow upscale to reach maximum vertical extent near local sunset, and weaken during the night. However, there is a distinct region of deep convection over and off the coast of Nayarit (20–23°N), in the Pacific Ocean, that remains active through the night and into the early morning, producing heavy rainfall and frequent lightning. Occasionally, the inner structure of these MCSs can move across the Gulf of California and reach the southern Baja California Peninsula. One particular long-lived, fast-moving MCS from July 23 and 24, 2014 was selected for in-depth analysis, because it was associated with weather conditions that included unusual precipitation and extreme winds. The MCS caused damage from sustained winds of tropical-storm strength and an intense gust front in the Los Cabos area, in the southern tip of the peninsula. This extraordinary MCS developed in the most unstable and humid environment recorded during the 1976–2018 period, and was supported by a collocated upper-level, inverted trough and a lower-troposphere tropical wave. We also found that the 10 most unstable conditions have all occurred after 2011, possibly indicative of a trend toward more frequent and favourable environments to spawn MCSs over the Gulf of California entrance.

KEY WORDS

extraordinary case study, mesoscale convection, observational analysis, warm season

1 | INTRODUCTION

A mesoscale convective system, hereafter referred to as an MCS, is an organized ensemble of thunderstorms with horizontal scale of hundreds of kilometres that generally persists for several hours (Maddox, 1980; Houze, 2004). Most MCSs develop over midlatitudes or the tropics with life cycles of several hours (Laing, 2015), but in a few exceptional cases, they may last more than 15 hr (Laing and Fritsch, 1997). The distribution, frequency, and tracks of MCSs have been compiled for Asia (Laing and Fritsch, 1993a; Laing and Fritsch, 2000), Africa (Laing and Fritsch, 1993b; Laing and Fritsch, 2000), Europe (Laing and Fritsch, 1997; Punkka and Bister, 2015), South America (Velasco and Fritsch, 1987; Garreaud and Wallace, 1997; Machado *et al.*, 1998; Salio *et al.*, 2007), and North America (Maddox and Howard, 1988; Valdés-Manzanilla *et al.*, 2005; Mejía *et al.*, 2015). These MCSs are active over the North American monsoon region which encompasses northwestern Mexico, the southwestern United States, and adjacent oceanic areas (e.g., Adams and Comrie, 1997; Higgins and Gochis, 2007), and are major contributors to the seasonal precipitation (Lang *et al.*, 2007; Nesbitt *et al.*, 2008; Wall *et al.*, 2012). However, they can also produce severe weather with heavy rainfall, strong winds, and frequent cloud-to-ground lightning (e.g., McCollum *et al.*, 1995) that may lead to significant societal impacts (Ray *et al.*, 2007; Raga *et al.*, 2014; Brooks *et al.*, 2019).

The core of the MCS activity tends to initiate over the Sierra Madre Occidental (SMO), a broad mountain range in western Mexico that is oriented from southeast to northwest (Figure 1). The SMO extends from east of Nayarit State, at roughly 20–23°N, through northern Sonora, 31–32°N, with mean elevation of 2,500 m and peaks up to 3,347 m (González-Elizondo *et al.*, 2012) across landscapes with deep canyons, steep slopes, and high plateaus that influence the low- to mid-level atmospheric flow (Nesbitt *et al.*, 2008). Annual rainfall over the SMO exceeds 400 mm (Mosíño Alemán and García, 1974) and, between July and September, most accumulations are received to the west of the maximum terrain elevations (Liebmann *et al.*, 2008); the primary rainfall sources are weather systems related to the North American monsoon, including MCSs, followed by tropical cyclones from the eastern Pacific (García and Trejo, 1994).

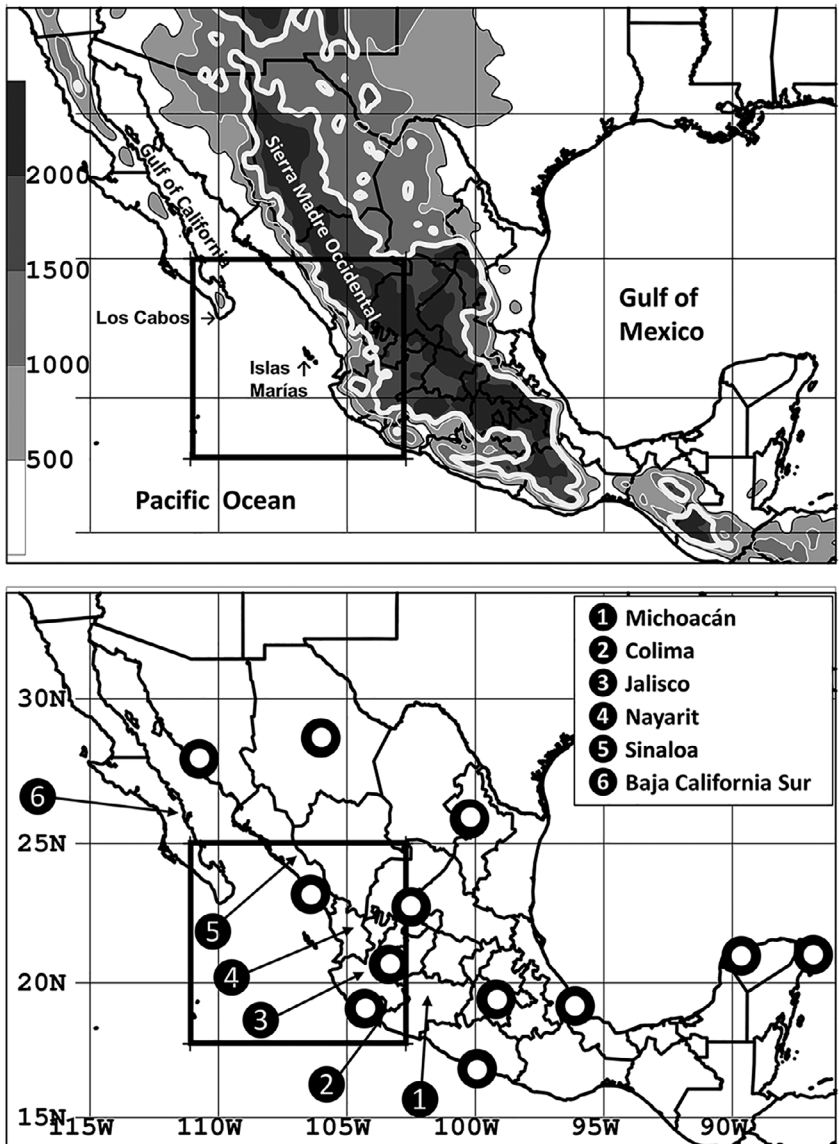
A distinct rainfall maximum greater than 500 mm has been detected off the west coast of Mexico and near the state of Nayarit (see Figure 1 for location). This maximum was first identified by Negri *et al.* (1993) and Negri *et al.* (1994), who noted that, from July through September, intense rainfall occurred close to sunrise.

Sea-breeze convergence over a concavity in the coastline was suggested as a mechanism to explain such a maximum, with a possible connection to MCS activity. The terrain configuration, warm near-shore seawater, and positive soil moisture anomalies are likely to control the rainfall patterns in this region (Brito-Castillo *et al.*, 2010). Moreover, a lightning climatology (Albrecht *et al.*, 2016) shows that Nayarit has one of the highest flash concentrations in Central America, the Caribbean, and North America. While the majority of Nayarit's activity occurs in the early evening, there are some flashes well after midnight, suggesting another connection to MCSs. The unique local maxima in convection, rainfall, and lightning were the motivations for our study.

Knowledge of MCSs in western Mexico emerged in the 1980s following systematic exploration of organized convection as detected from geostationary satellites. In a pioneering study, Velasco and Fritsch (1987) reported MCSs close to the coast not far from the state of Nayarit, with clusters inland immediately west of the SMO and offshore over the Gulf of California. Howard and Maddox (1988a) examined typical life cycles of MCSs from the 1980–1987 period, including track and duration; they found a distinct group of nocturnal systems that initiated over western Jalisco, Nayarit, and southern Sinaloa in July and August. They had an average duration of 15 hr with early stages near sunset, maximum extent by sunrise, and dissipation the morning over the southern gulf. These authors also found that several systems continued their growth and motion, eventually, into the Baja California Peninsula. The extended lifetime of convection, from the late afternoon into the night, is associated with long-lived MCSs (Howard and Maddox, 1988b). Farfán and Zehnder (1994) noticed that MCSs with slow forward motion ($<4.6 \text{ m s}^{-1}$) were primarily in the southern gulf while faster MCSs occurred along the mainland coast.

Field campaigns, such as the Southwest Area Monsoon Project (Meitin *et al.*, 1991) and the North American Monsoon Experiment (Higgins and Gochis, 2007), have contributed significantly to better understand the behaviour of deep convection in western Mexico (Brooks *et al.*, 2019). For example, radar observations were used to document the stratiform and convective structures of MCSs (Rowe *et al.*, 2011; Rowe *et al.*, 2012). Lang *et al.* (2007) found that convection grew upscale over the SMO and either moved westward to the gulf or northwestward along the mainland coast; easterly winds at 700 hPa, along with enhanced vertical wind shear, tend to support MCS organization and precipitation features. However, there remains a gap in the climatology of MCSs that propagate from the mainland coast, westward across the gulf, and arrive in Baja California; our study aims to help fill such a gap.

FIGURE 1 Topography of Mexico, elevations above 500 m are shaded with the 1,500-m contour given by the thick line (top panel). Locations of six Mexican states (numbered black dots) and upper-air network (white dots) that were available from July 20 to 28, 2014 (bottom panel). Black boxes outline the study area



Few studies, other than those from Howard and Maddox (1988a), Farfán and Zehnder (1994), Lang *et al.* (2007), and Nesbitt *et al.* (2008), have addressed MCS development over the Gulf of California entrance. Our goals are thus (a) to create a climatology to examine MCS characteristics over northwestern Mexico from remotely sensed data, and (b) analyse one extreme event in which an MCS propagated across the gulf, and resulted in severe impact in Los Cabos. The latter is a populated area in the southern tip of Baja California (see Figure 1). We also discuss the synoptic- and meso-scale environment in which the gulf entrance MCSs are embedded, so their impacts (i.e., rainfall and wind) in the peninsula can be placed in a climatological perspective.

The remainder of this article is divided as follows: Section 2 describes the data sources and methodology.

The analysis of convection and precipitation from the 2009–2018 period, along with a selection of MCSs, are presented in Section 3. A detailed analysis of the extraordinary MCS from July 2014, including the evolution of key features at the surface and upper levels, are discussed in Section 4. A summary and concluding remarks are provided in Section 5.

2 | DATA AND METHODS

Infrared (11.5–13.7 μm) brightness temperature from Geostationary Operational Environmental Satellites (GOES; Goodman *et al.*, 2017), located at 135°W, was analysed in this study with GOES-11 from 2009 through 2011 and GOES-15 from 2012 through 2018. Each image has 4-km (line) and 8-km (element) horizontal spacing, is

available at 30-min intervals, and is operationally calibrated to determine cloud-top temperature. The data from 2009 to 2018 were used to identify MCS structures over northwestern Mexico, the southwestern United States, and the eastern Pacific Ocean during July–September.

In addition to allowing us to place MCS events in a historical context, the GOES imagery allowed us to build a detailed climatology of deep convection. Timing, structure, and intensity of convection are represented by the 3-hourly frequency of cloud-top temperature lower than -38°C . This temperature threshold places cloud tops roughly 10–11 km above mean sea level and has been used to identify convection features in other studies over the region of interest (e.g., Douglas *et al.*, 1993; Negri *et al.*, 1993; Stensrud *et al.*, 1995; Gebremichael *et al.*, 2007; Mejia *et al.*, 2015).

Estimations of accumulated rainfall were analysed using products from the Global Precipitation Measurement (GPM; Huffman *et al.*, 2019) Mission Integrated Multi-satellite Retrievals, version 6. These products are available at 30-min intervals and $0.1^{\circ} \times 0.1^{\circ}$ resolution in the horizontal; rainfall estimates come from a combination of passive microwave sensors and imagery from geostationary satellites. The estimates were also used to create a monthly climatology (2009–2018) of warm-season rainfall. Just as with the GOES dataset, this climatology serves to place individual MCS events in a regional context.

Lightning activity can provide useful insight into the structure of an MCS (e.g., Dotzek *et al.*, 2005). Here, we examined the evolution of flashes using lightning observations from the World Wide Lightning Location Network (WWLLN), managed by the University of Washington. The WWLLN information consists of date, time, and location of flashes. Higher lightning flash density implies more intense updrafts within an MCS (e.g., Zipser *et al.*, 2006; Lang *et al.*, 2017). One of the advantages of the WWLLN is the nearly continuous data, with respect to time, to characterize short-duration convective phenomena (e.g., Virts and Houze, 2016; Barrett *et al.*, 2017).

A network of surface automated stations operated by Mexico's Secretaría de Marina, Servicio Meteorológico Nacional (SMN), and from the airport authority is used to examine changes in weather conditions. Records include 10-m sustained winds and peak gusts, 2-m temperature and relative humidity, accumulated precipitation, and barometric pressure from Islas Marías and the coastal plains in Los Cabos (see Figure 2 for locations). We also analysed upper-air soundings released by SMN in Manzanillo, Colima (19.05°N , 104.32°W , 3 m) and other nearby Mexican stations. From each sounding, we

extracted the following derived parameters: mixed-layer convective available potential energy (CAPE), mixed-layer convective inhibition (CIN), total precipitable water (PW) in the vertical column, and lifted index (LI) at 500 hPa. The sounding observations were provided by the Integrated Global Radiosonde Archive (Durre *et al.*, 2006).

The three-dimensional structure of the environmental flow over much of North America was explored with the aid of the Fifth Generation ECMWF atmospheric reanalysis of the global climate (ERA5; Hersbach *et al.*, 2020) at 31-km horizontal spacing and hourly updates. We examined CAPE, PW, and geopotential heights at isobaric levels (200, 500, 700, and 850 hPa) to identify circulations associated with nine of the most unstable days in the Gulf of California entrance. Additionally, geopotential height anomalies during one extraordinary MCS event, from July 24, 2014, were calculated based on a 10-year ERA5 climatology (2009–2018).

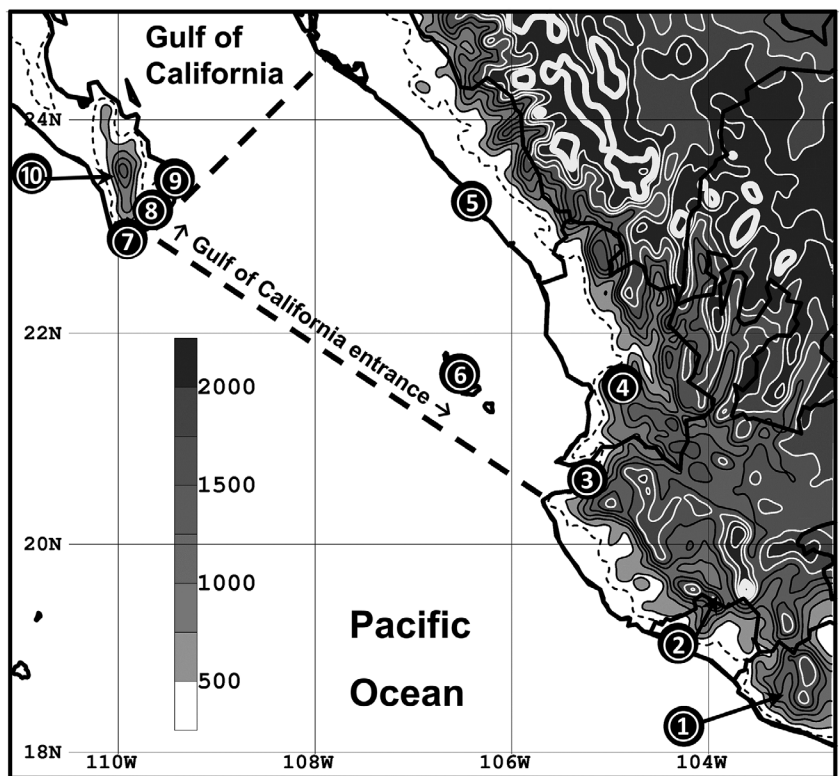
3 | CLIMATOLOGICAL RESULTS: 2009–2018

3.1 | Deep convection

Patterns of convective clusters are derived from the GOES imagery for July through September 2009–2018 (Figure 3). The diurnal cycle of cloud tops colder than -38°C starts at 1800 UTC (1200 LT) and is examined every 3 hr. In a composite sense, convective cells tend to develop by 2100 UTC over Michoacán and Jalisco states and, also, along portions of the SMO where terrain elevations exceed 2,000 m. Farther north in the mainland of Mexico, another large region of deep convection appears over the SMO, with maximum intensity over southeastern Sonora as documented by Douglas *et al.* (1993), Negri *et al.* (1993), and Stensrud *et al.* (1995).

The initial cells grow upscale into organized systems and move westward to reach a maximum horizontal extent near sunset (0000–0300 UTC). At midnight, there is a distinct region of convection over Nayarit which, while weakening, tends to slowly move westward into the Pacific (0900–1200 UTC). This feature is consistent with a 0600–1200 UTC maximum in lightning activity documented by Holle and Murphy (2015) over the southeastern Gulf of California. In our climatology, there is minimal deep convection over the gulf entrance and the Baja California Peninsula as cloud tops reaching -38°C are much less frequent there. Additional analysis indicates that, in the early afternoon (2100–2300 UTC), cloud tops in the range of -10 to 0°C (5–7 km above mean sea level) occur over the southern peninsula. The distribution

FIGURE 2 Terrain elevations (m) and relevant features in the study area. The 250-m elevation is given by the thin, dashed line to outline the coastal plains, and shading is for terrain elevations above 500 m. White lines are elevations at and above 1,500 m; thick line is the 2,500-m level. The dashed polygon and the eastern coast define the Gulf of California entrance. Specific locations mentioned throughout the article are: ① Cerro las Conchas, Michoacán, ② Manzanillo, Colima, ③ Puerto Vallarta, Jalisco, ④ Tepic, Nayarit, ⑤ Mazatlán, Sinaloa, ⑥ Islas Marías, Nayarit, ⑦ Cabo San Lucas, Baja California Sur, ⑧ Los Cabos international airport, ⑨ Cabo Pulmo, Baja California Sur, and ⑩ Sierra la Laguna, Baja California Sur



of these convection features is consistent with the results of Nesbitt *et al.* (2008) for July–August 2004.

From the above, we conclude that there are two hot spots of deep convection associated with MCS development in northwestern Mexico. One spot is confined to the western foothills of the SMO and coastal areas close to the Gulf of California (from 0000 to 0600 UTC). There is a secondary spot over Nayarit (from 0300 to 0600 UTC) that remains active overnight (from 0900 to 1200 UTC) over the adjacent Pacific Ocean and east of Islas Marías. The horizontal scale of this spot, less than 250×250 km, suggests that the corresponding MCSs are likely to be stationary or follow relatively slow motion as previously found by Farfán and Zehnder (1994), Lang *et al.* (2007), and Nesbitt *et al.* (2008).

3.2 | Accumulated precipitation

The monthly evolution of GPM-derived precipitation from 2009 to 2018 was computed for a large area covering northern Central America (poleward of 13°N), Mexico, and a portion of the United States (equatorward of 37°N). Early in the warm season (not shown), May has a precipitation maximum with an average accumulation greater than 400 mm in western Guatemala, more than 1,500 km away from northwestern Mexico and, in June, the maximum is located over the Gulf of Tehuantepec.

In July (Figure 4), an area in excess of 200 mm is located close to Nayarit while a distinct maximum develops over northwestern Mexico off northern Sinaloa. Consistent with the composite pattern of deep convection (Figure 3), August displays a well-defined maximum above 400 mm between coastal Nayarit and Islas Marías over the Pacific Ocean. This maximum is larger than the accumulations over the northern SMO where peaks are between 275 and 325 mm. This offshore maximum remains in place through September. In October, like May and June, the rainfall distribution is limited to areas over southern Mexico and Central America. These changes in the distribution of rainfall patterns are broadly consistent with the seasonal cycle of convection reported elsewhere (e.g., Cortez Vazquez, 1999), and the July–September climatology of rainfall by Negri *et al.* (1994).

Records from an SMN rain-gauge network in Nayarit have annual averages in the range of 1,000–1,500 mm that tend to peak in July or August. These spatial and temporal features are consistent with the results of previous studies (Reyes and Cadet, 1988; García and Trejo, 1990; García-Oliva *et al.*, 1991; Vidal-Zepeda and Hernández Cerdá, 1992; Gochis *et al.*, 2009; Brito-Castillo *et al.*, 2010 and Perdigón-Morales *et al.*, 2018). In particular, Palacios-Hernández *et al.* (2012) found that stations along the coast of Nayarit have a sharp peak in August and annual average (from 1922 to 1989) in the range of

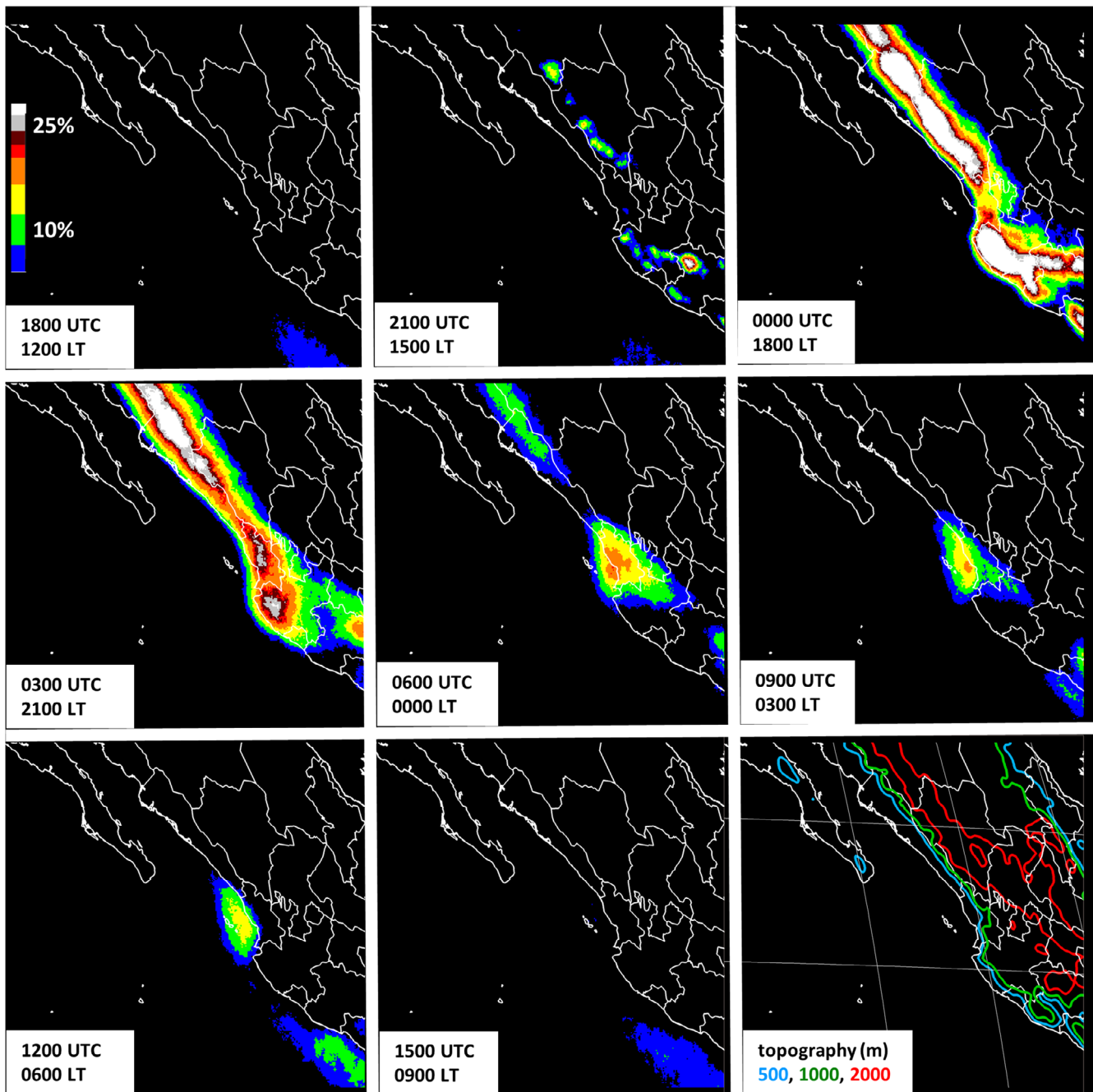


FIGURE 3 Frequency (percentage) of cloud tops that reached at least -38°C in the GOES infrared imagery during the period 1 July–30 September from 2009 through 2018. The display area is bounded by 17°N , 28°N , 98°W , and 115°W . Times start at 1800 UTC (1200 local time, LT) with 3-hourly increments to end at 1500 UTC (0900 LT). The 500-, 1,000-, and 2000-m contours of terrain elevation are also given [Colour figure can be viewed at wileyonlinelibrary.com]

1,140–1,427 mm. In contrast, Islas Marías (100–150 km to the west of the coast) only records 520 mm per year, with a September maximum associated with eastern Pacific tropical cyclones; this is comparable with the 564-mm mean from Vidal-Zepeda and Hernández Cerdá (1992). These observations support the satellite-derived enhanced area of rainfall over the Pacific (Figure 4); in fact, the sharp contrast between the coastal

and offshore island rainfall characteristics motivated our study of MCSs in this area.

3.3 | MCS selection

In this section, we examine weather events associated with (a) convective development in July, when tropical

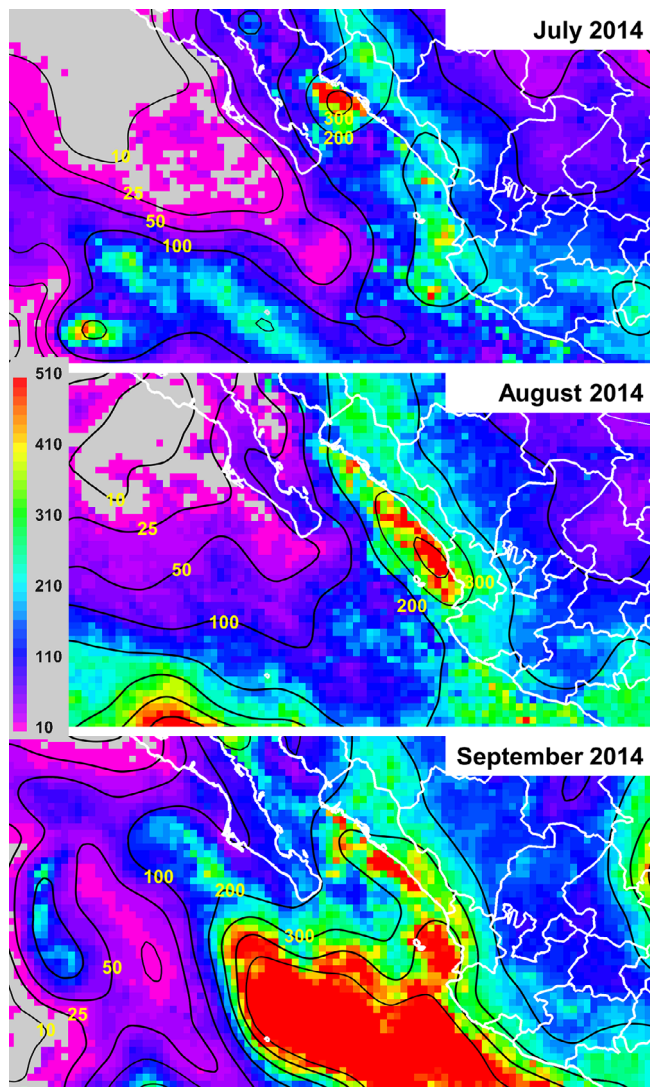


FIGURE 4 Average of monthly rainfall (mm) from GPM for 2009–2018, from July (top), August (Centre), and September (bottom). Shading is for accumulations above 10 mm; black lines are for a selection of contours up to 500 mm. Note a rainfall maximum exceeding 400 mm off the coastal region of Nayarit in August and September [Colour figure can be viewed at [wileyonlinelibrary.com](#)]

cyclones do not play a substantial role; (b) MCSs that developed over the Gulf of California entrance off Colima, Jalisco, or Nayarit; and (c) severe conditions (rainfall and wind) with impacts in Los Cabos, Baja California Sur. Baja California is an extension of the Sonoran desert of North America (Warner, 2004) where the main precipitation events are tropical cyclones (e.g., Latorre and Penilla, 1988), convective systems (García and Trejo, 1994), or a combination of both (Farfán, 2005).

The atmospheric environment associated with gulf entrance MCSs is derived from 351 Manzanillo

TABLE 1 Ten days with highest convective available potential energy (CAPE, J kg^{-1}) at 0000 UTC from upper-air observations in Manzanillo, Colima, for the period 1–31 July, from 1976 through 2018

Rank	CAPE	PW	LI	Date (year/day)
1	7,191	64	-5	2014/16
2	6,262	67	-3	2014/18
3	6,003	57	-10	2014/24
4	5,331	51	-8	2014/23
5	5,054	56	-6	2014/11
6	4,990	49	-2	2014/31
7	4,795	50	-5	2015/19
8	4,607	52	-8	2012/27
9	4,549	55	-9	2015/28
10	4,329	56	-8	2012/23
Average	1,256	39	-6	1976–2018

Note: The corresponding estimates of total column precipitable water (PW, mm) and lifted index (LI, $^{\circ}\text{C}$) at 500 hPa, at the same date and time, are included. Averages are from all the available records in the above period. The July 24, 2014 record and period averages are indicated in bold.

soundings, from the 1976–2018 period, at 0000 UTC. Table 1 allows to determine that:

- Between 2012 and 2018, CAPE had the top 10 values in the range of 4,329–7,191 J kg^{-1} .
- Six of the all-time highest CAPE values ($>4,990 \text{ J kg}^{-1}$) were on and July 11, 16, 18, 23, 24, and 31, 2014.
- In the top-10 days, CAPE exceeded the average from MCSs over the northern SMO ($2,160 \text{ J kg}^{-1}$; Smith and Gall, 1989) and the typical values from precipitation systems in the southern Gulf of California and west of the SMO ($1,539\text{--}1,687 \text{ J kg}^{-1}$; Lang *et al.*, 2007).

On July 24, 2014, CAPE reached the third highest value ($6,003 \text{ J kg}^{-1}$) in the 1976–2018 period; furthermore, there were extreme values of PW (57 mm) and LI (-10°C), well above long-term averages of 39 mm and -6°C , respectively. When soundings from August and September are included, July 24, 2014 ranks fifth with respect to the highest CAPE. Therefore, on this date, the regional environment was exceptionally favourable for intense deep convection if it could form.

Figure 5 shows the distribution of cloud-top temperature at 0300 UTC (2100 LT) for the highest-CAPE dates in July, except for July 24, 2014, which is shown separately. We selected the 0300 UTC imagery, 3 hr after the nominal sounding release, to identify if deep convection (cloud-top temperature $<-38^{\circ}\text{C}$) had developed near the Gulf of California entrance; images at 0600, 0900, and

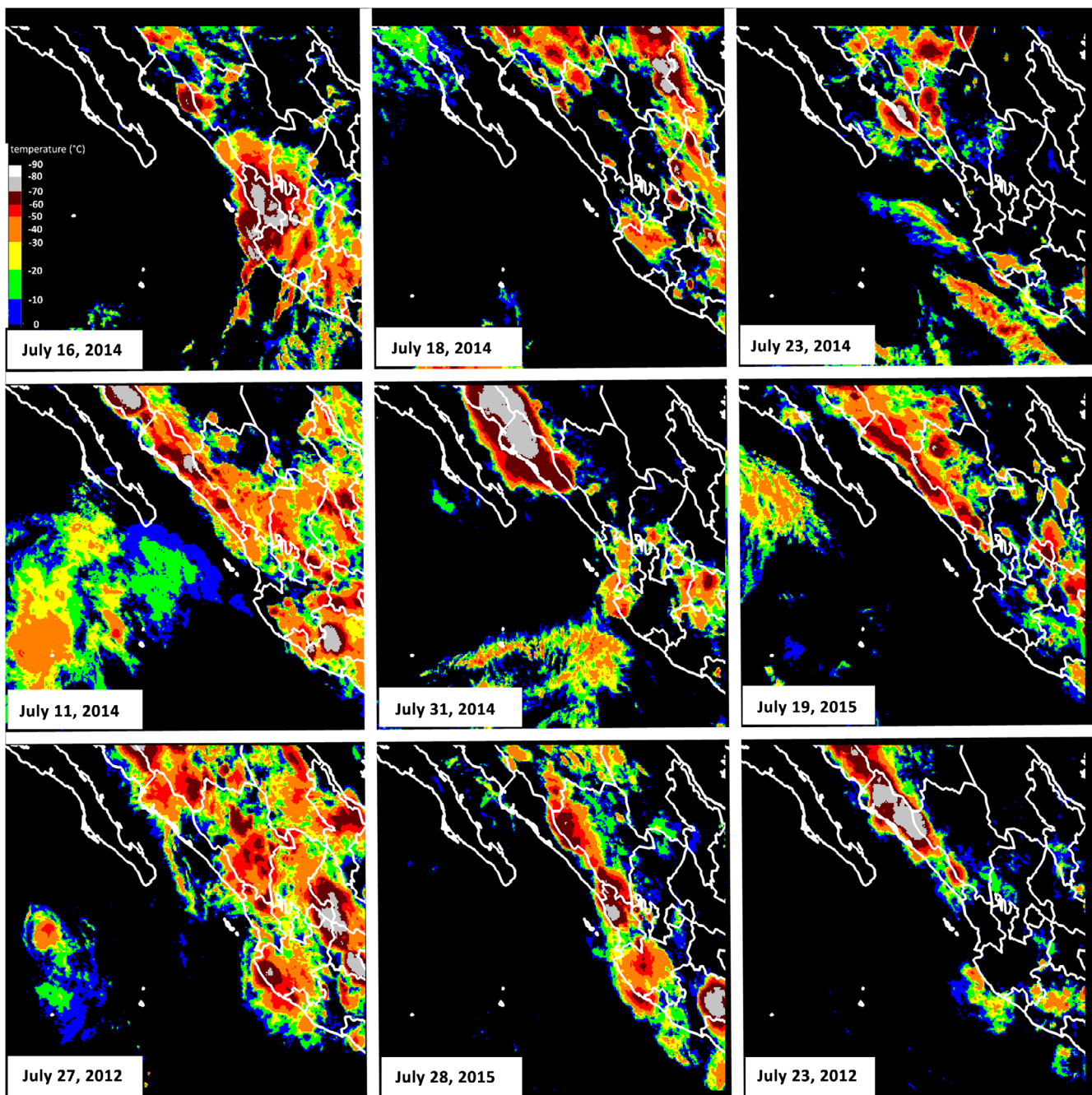


FIGURE 5 Cloud-top temperature ($^{\circ}\text{C}$) from GOES-15 infrared imagery at 0300 UTC (2100 LT) for nine dates with the largest values of CAPE (see in Table 1), excluding July 24, 2014. The vertical bar (a) indicates a calibrated scale from 0°C through -90°C [Colour figure can be viewed at wileyonlinelibrary.com]

1200 UTC were also inspected but are not shown. CAPE exceeds $4,000 \text{ J kg}^{-1}$ on every one of these dates, and there is deep convection inland or over coastal areas of Colima, Jalisco, and Nayarit (except for July 19, 2015). However, despite having deep convection and high CAPE, only the MCSs observed on 16 and July 24, 2014 were able to cross the gulf entrance through Islas Marías and, eventually, arrive at Los Cabos. Since the distance between these locations is $\sim 350\text{--}400 \text{ km}$, the presence of

relatively high-CAPE values alone may not be sufficient to generate a moving system that goes as far as Baja California.

To identify synoptic-scale patterns of the flow present during the development of gulf entrance MCSs, composite geopotential heights from the highest-CAPE days in Table 1 (except July 24, 2014) are shown in Figure 6. Additionally, to find relevant differences with the long-term heights, we computed anomalies (not shown) from

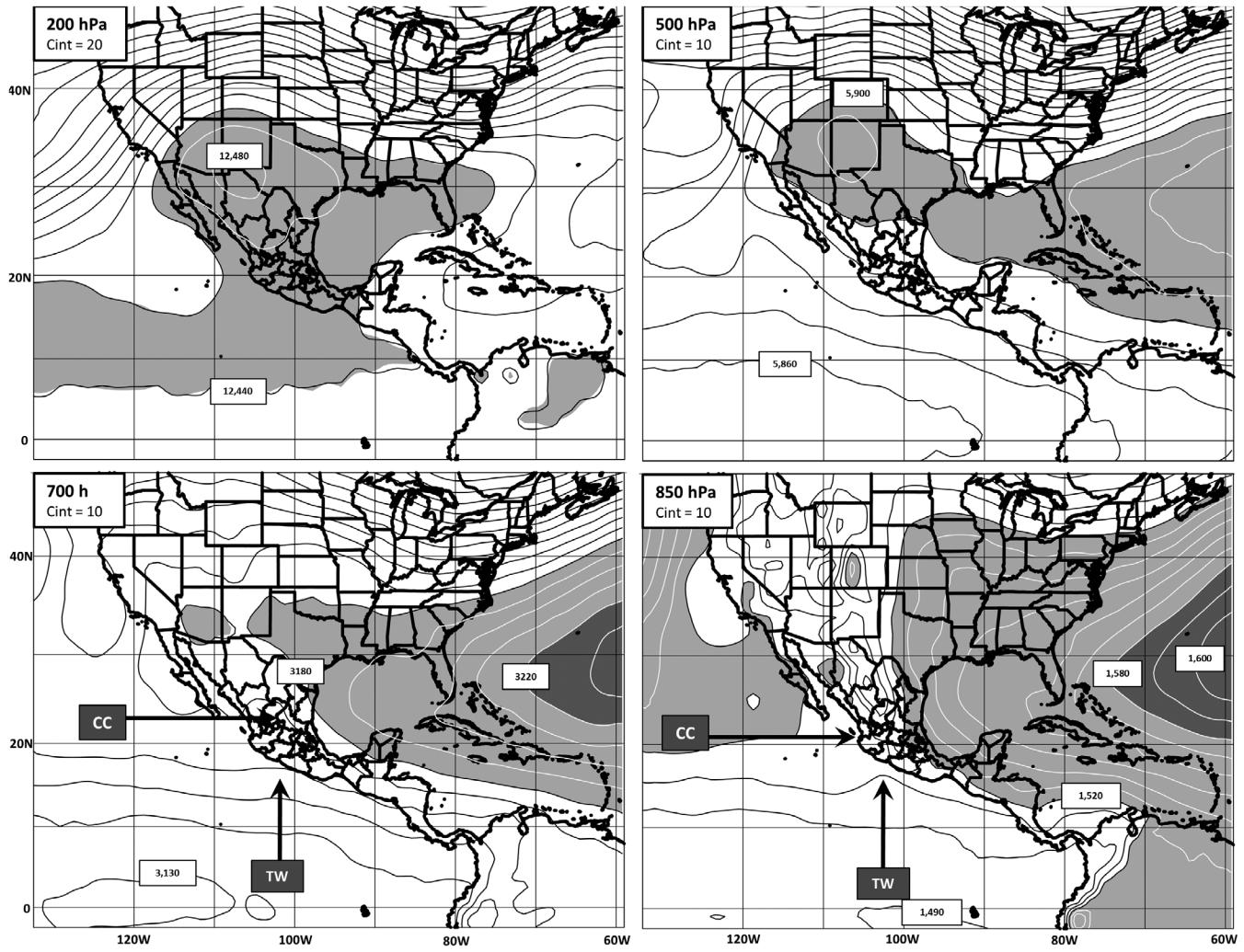


FIGURE 6 Composite fields at 0000 UTC of the nine highest CAPE days in Table 1 (excluding July 24, 2014). Average geopotential height (lines, m) at four isobaric levels are from the ERA5 analyses at the 200-, 500-, 700-, and 850-hPa levels. Selected contours are labelled and shaded; Cint gives the corresponding contour interval in m. A cyclonic circulation (CC) and a tropical wave (TW) are labelled at 700 and 850 hPa

the 2009–2018 average. On days with extreme CAPE along the coast of western Mexico, a stronger-than-normal upper-level (200 and 500 hPa) anticyclonic circulation tends to be located over northern Mexico and the southwestern United States. In contrast, negative 200-hPa height anomalies are over the northern Gulf of Mexico and the Pacific off Baja California. The 500-hPa anticyclone is displaced to the north, and this configuration would allow mid-level southerly flow over northwestern Mexico to steer MCSs toward the northern gulf and western Sonora. In addition to the features at 200 and 500 hPa, Figure 6 shows evidence of a cyclonic circulation at 700 and 850 hPa (feature CC) over southwestern Mexico, and a tropical wave off Michoacán (feature TW). In the next section, the above features are compared to actual fields from the MCS on July 24, 2014.

To determine a baseline of regional impacts from rainfall accumulations above 25 mm (1937–2018) or sustained winds (2000–2018) above 10 m s^{-1} , we inspected the available observations from two surface stations in Cabo San Lucas (see Figure 2 for locations). Table 2 shows that the seventh-largest accumulation in the 82-year record is from the MCS on July 24, 2014, and this accumulation was exceeded only by events associated with tropical cyclones or other MCSs developing over the gulf entrance in 1979 and 1990. The highest sustained wind speed (and peak gust) in the historical record came, again, from the July 24, 2014 MCS although the period of record was shorter for wind measurements, only 19 years. We also found events of intense, nocturnal westerly flow with speed up to 17.9 m s^{-1} (21.2 m s^{-1} peak) and they are termed “local” in Table 2; these events are not

TABLE 2 Top 10 records from two SMN surface stations in Cabo San Lucas, Baja California Sur

Rainfall (mm)				Wind (m s^{-1})			
Rank	Accumulation	Date ^a	Source ^b	Rank	Sustained/gust	Date	Source ^b
1	113	1954/15–16	TC#3	1	26.2/34.7	2014/24	MCS
2	86	1950/3–4	TC#2	2	24.1/31.9	2006/24	Emilia
3	63	1950/4–5	TC#2	3	17.9/21.2	2008/03	Local
4	49	1979/28–29	MCS	4	14.1/16.3	2008/03	Douglas
5	41	1990/6–7	MCS	5	14.0/16.1	2011/11	Local
6	38	1948/18–19	N/A	6	12.4/15.2	2012/01	Local
7	29	2014/23–24	MCS	7	12.4/16.1	2017/01	Local
8	28	2006/22–23	Emilia	8	12.4/15.3	2008/04	Douglas
9	27	1970/18–19	Helga	9	12.2/13.7	2011/23	Dora
10	27	2006/23–24	Emilia	10	12.1/13.9	2011/26	MCS

Note: Events are ranked according to the maximum rainfall accumulation (mm) for the period 1–31 July, from 1937 through 2018 (left columns), and according to the maximum sustained wind speed (m s^{-1}) for 1–31 July, from 2000 through 2018 (right columns). Sustained wind speed and corresponding gust (m s^{-1}) are from 0000–2350 UTC records, updated every 10 min. The July 23 and 24, 2014 records are indicated in bold. Local is explained in the text.

Abbreviations: MCS, mesoscale convective system; N/A, not available.

^aYear/days; as reported from records for a 24-hr period beginning at 1500 UTC.

^bTC#XX is the XXth tropical cyclone for seasons prior to 1960.

directly associated with convective storms and, to our knowledge, they have not been reported in the literature yet.

4 | EXTRAORDINARY CASE: JULY 24, 2014

In this section, we provide a discussion of the extraordinary MCS by examining remote sensing and in-situ datasets. As seen from Table 2, when compared to other July events, this MCS brought moderate rainfall (29 mm) and strong winds (26.2 m s^{-1} sustained, 34.7 m s^{-1} peak gust) to Cabo San Lucas.

4.1 | Remote sensing datasets

Examination of the GOES imagery from 23 to 24 July provides insights on the structural features of convection that developed over western Mexico, the Gulf of California, and Pacific Ocean (Figure 7). The first convective cells formed by 1800 UTC 23 July over Cerro las Conchas, a small mountain range in Michoacán (see Figure 2 for location). During the next 6 hr, cells moved parallel to the coast of Colima and Jalisco, with cloud-top temperature colder than -70°C equivalent to a height more than 16 km per Manzanillo's upper-air observation at 0000 UTC 24 July. The MCS intensified as it crossed the coast

of Jalisco and moved into the ocean. Between 0300 and 0900 UTC, cloud tops were colder than -70°C over part of the gulf entrance and, from 1200 to 1500 UTC, similar cloud tops covered the southern peninsula including eastern Los Cabos.

The spatial distribution of lightning flashes provides information on the internal structure of convective cells (Deierling and Petersen, 2008) and it is especially valuable over areas of northwestern Mexico devoid of observations (e.g., Adang and Gall, 1989; Smith and Gall, 1989). As shown in Figure 8, in the early stages, few flashes were detected inland in agreement with the distribution of relatively warm cloud tops (Figure 7). The MCS became better organized, with a large area of flashes near the coast of Colima, Jalisco, and Nayarit from 0000 to 0559 UTC 24 July. The Puerto Vallarta (MMPR) and Tepic (MMEP) international airports reported lightning flashes during the period 0300–0800 UTC. As the MCS moved over the gulf entrance, the electrical activity was off the coast of southern Sinaloa and, between 1200 and 1500 UTC, the concentration of flashes reached Los Cabos.

A closer inspection of the available observations suggests a linear structure associated with deep convection, in agreement with findings from other MCSs (e.g., Barnes and Sieckman, 1984; Bluestein and Jain, 1985; Smith and Gall, 1989; LeMone *et al.*, 1998). Figure 9 shows a line of convection over the gulf entrance from 15-min flashes and reflectivity from an SMN radar

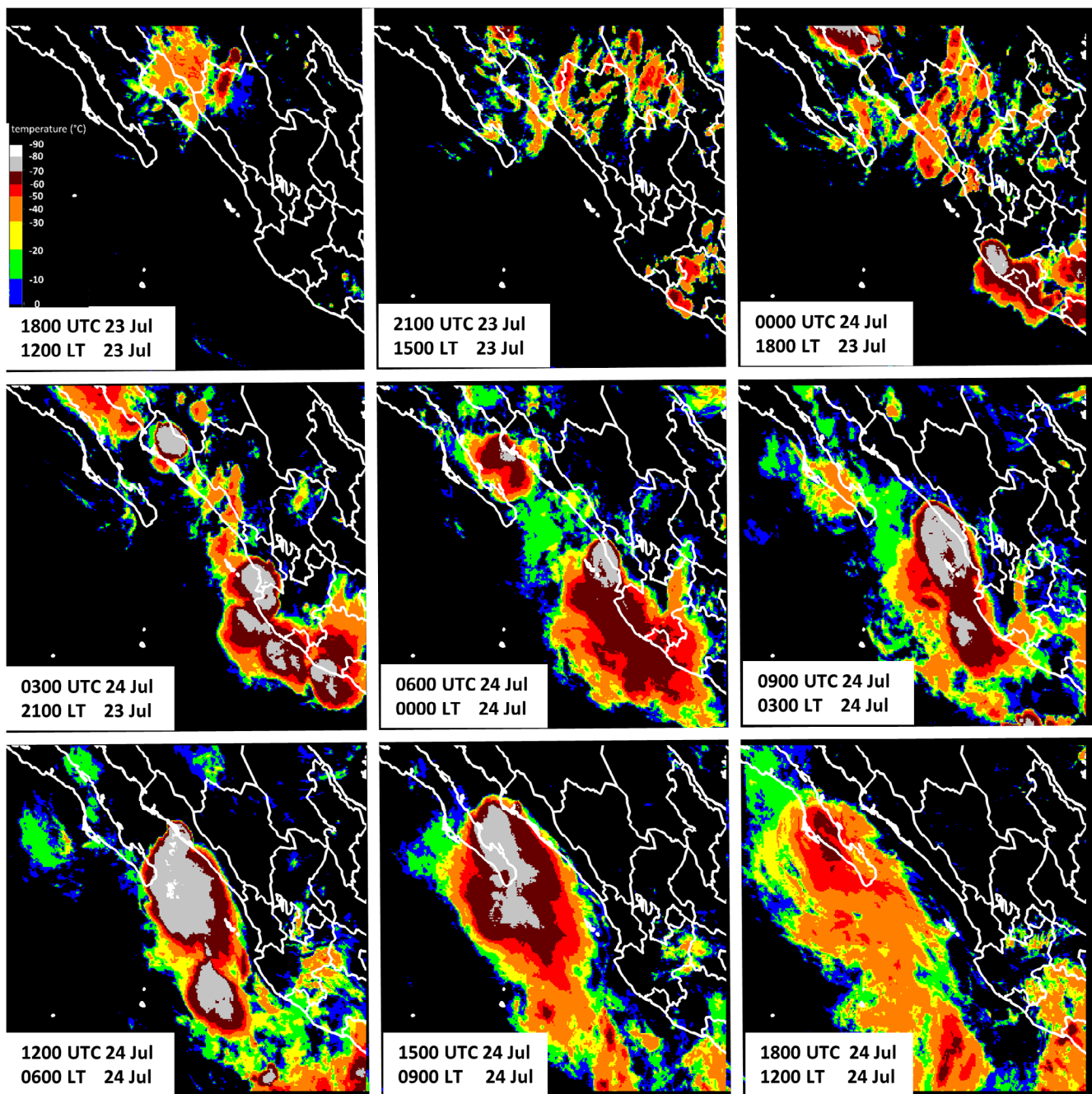


FIGURE 7 As in Figure 5 but for cloud-top temperature ($^{\circ}\text{C}$) from GOES-15 infrared imagery for 1800 UTC 23 July through 1800 UTC 24 July 2014 with 3-hourly increments. Local times (LTs) are also given. The vertical bar (a) indicates a calibrated scale from 0°C through -90°C [Colour figure can be viewed at wileyonlinelibrary.com]

in Guasave, Sinaloa. Maximum reflectivity (30–50 dBZ) is located over the gulf and, by 1200 UTC, the line's eastern edge reached the coast of Sinaloa, consistent with the distribution of lightning flashes (Figure 8) and cloud tops (Figure 7). The radar also depicts a small area of stratiform precipitation, under 20 dBZ, surrounding the reflectivity maxima, characteristic of weakening MCSs (Houze, 2004). This linear feature kept moving across the southern gulf and remained well defined until 1800 UTC

(not shown) when the western edge of the convection line vanished.

To contextualize the structure of the extraordinary MCS, all flashes from July, August, and September 2014 are examined; their distribution is shown in Figure 10 and summarized in Table 3. The analysis follows a classification with four daily periods to compare with other events in the study area. In general, as in Holle and Murphy (2015), August tends to be slightly more active

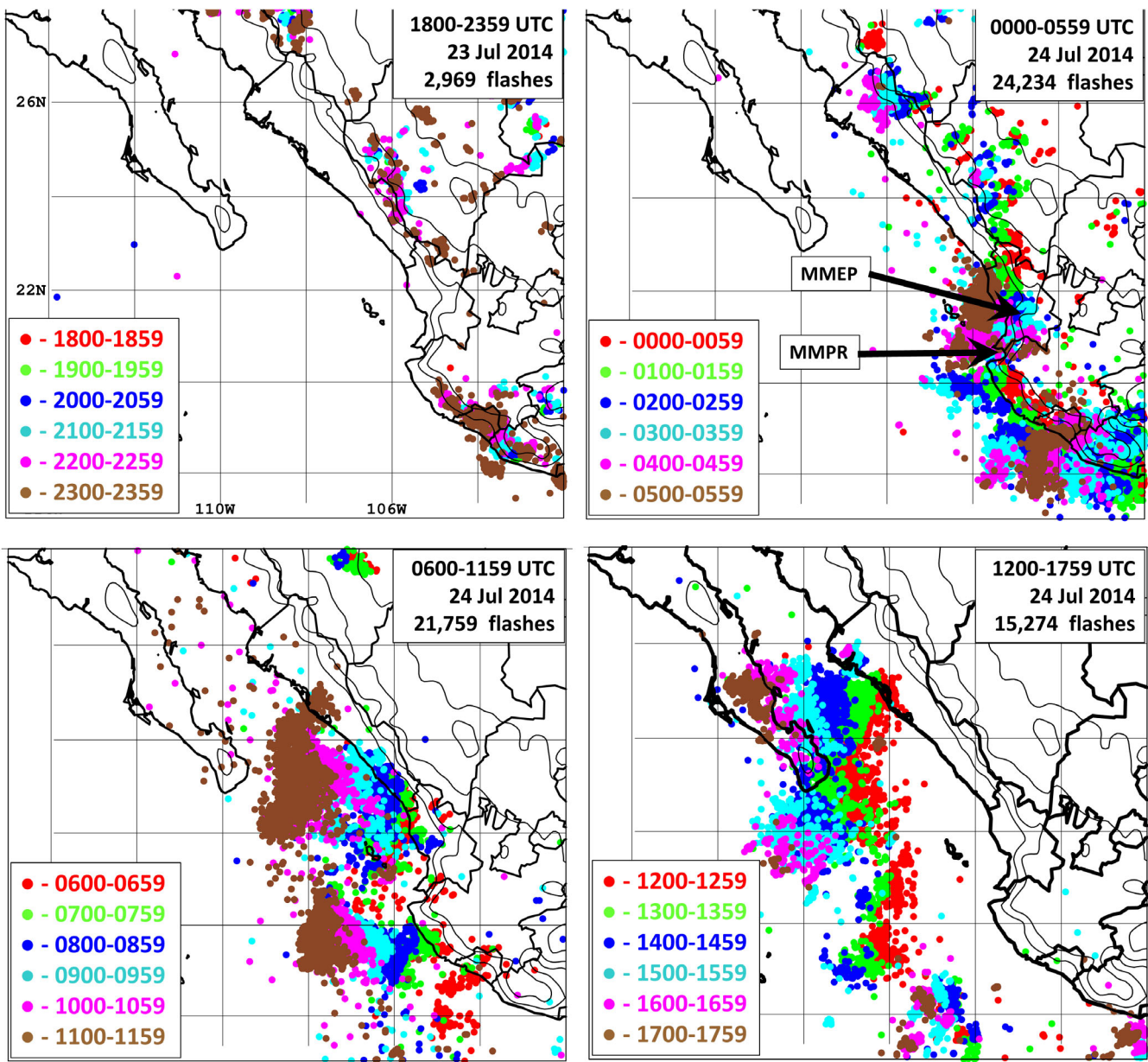


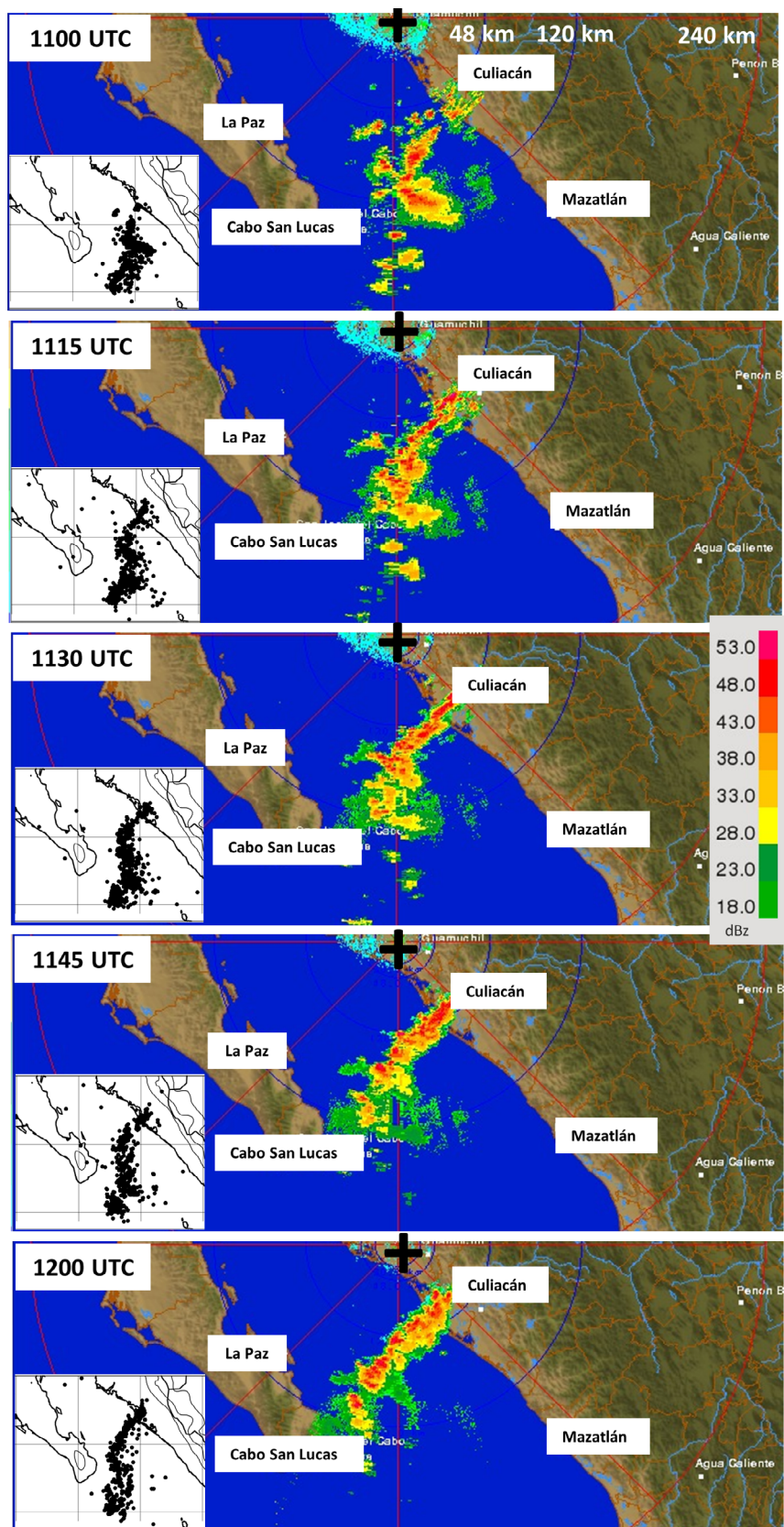
FIGURE 8 Lightning flash counts from the WWLLN network, classified into hourly intervals from 1800 UTC 23 July through 1759 UTC 24 July 2014. Time range, date, and total number of flashes per 6-hr periods are indicated in the upper-right corner of each panel. The 500-, 1,000-, and 2000-m contours of terrain elevation are given in black lines. Approximate location of Puerto Vallarta (MMPR) and Tepic (MMEP) airports is shown [Colour figure can be viewed at wileyonlinelibrary.com]

than July and September when fewer MCSs are detected (e.g., Valdés-Manzanilla, 2015; Vega-Camarena *et al.*, 2018). During the evening, night, and morning periods, 24 July was the most active and among the top five to seven most active days over the extended period July–September. In contrast, the flash count from the previous afternoon (23 July) in Table 3 was among the least active periods, ranked in 29th (77th) place for July (July–September), and consistent with reduced convection in the GOES imagery (Figure 7). In summary, the 24 July MCS stands out as a unique event when

compared with other days of July and the warm season of 2014.

Rainfall estimates from GPM demonstrate that between 1800 UTC 23 July and 0000 UTC 24 July (Figure 11), limited accumulations (<20 mm) were associated with few cells (Figure 7) and lightning flashes (Figure 8) over the coast of Michoacán and Colima. Accumulations exceeding 30 mm occurred later over the gulf entrance, southeast of Islas Marias (0000–0600 UTC 24 July); then, the rainfall is seen off the Sinaloa coast from the MCSs developing to the north and west of the

FIGURE 9 Reflectivity (dBZ) from the Guasave, Sinaloa, radar every 15 min for the period 1100 UTC through 1200 UTC 24 July 2014. The radar is at the plus symbol with 48-, 120-, and 240-km radii label in the top panel. Black dots are lightning flashes from the WWLLN network at 15-min intervals. Selected cities are labelled in white boxes [Colour figure can be viewed at wileyonlinelibrary.com]



islands (0600–1200). The gulf entrance received significant accumulations between 60–100 mm, with two distinct maxima near Los Cabos: one to the south and

another to the east (1200–1800). These areas are associated with numerous lightning flashes and a reflectivity line from the Guasave radar (Figure 9). Note that, on the

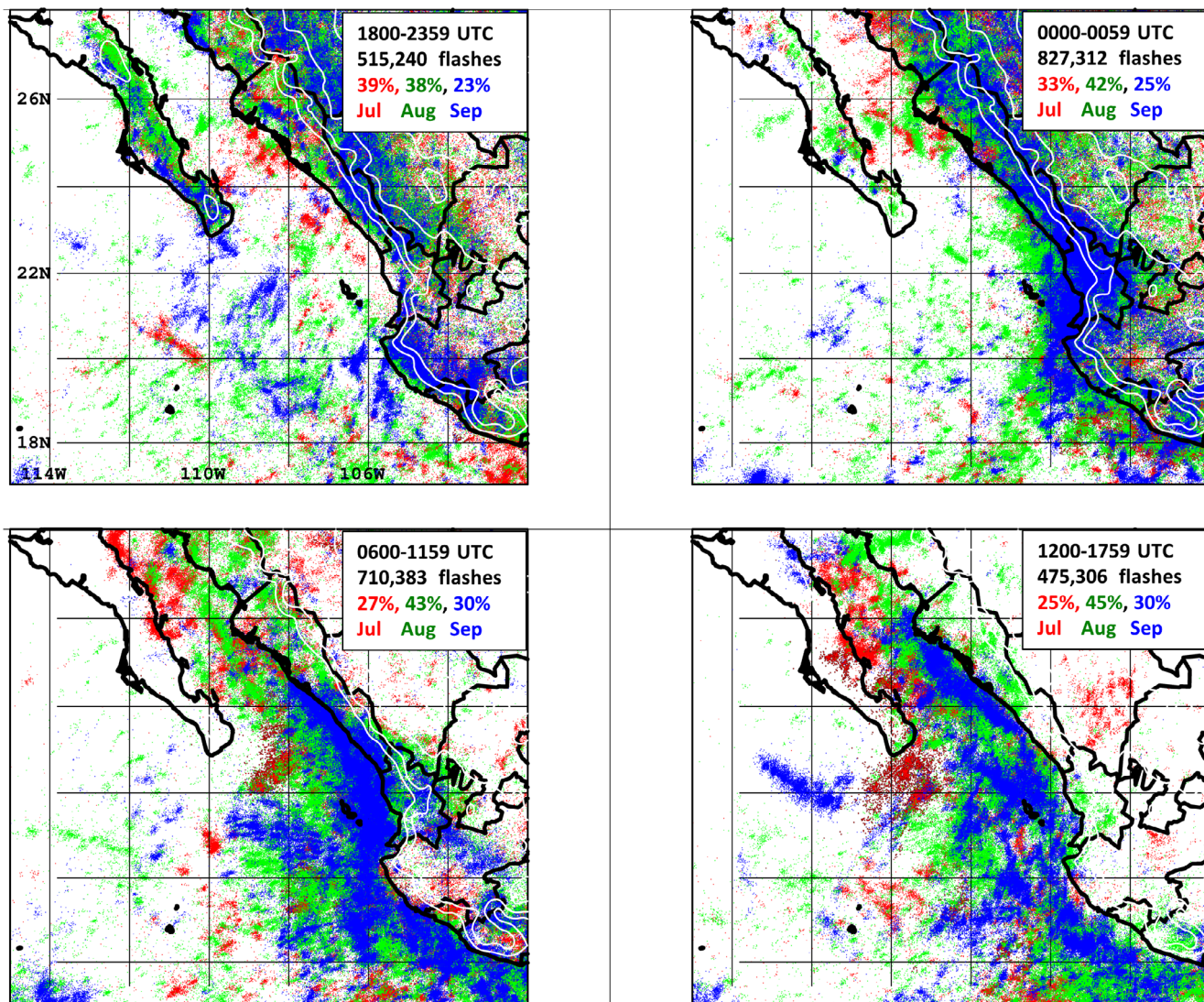


FIGURE 10 Distribution of lightning flashes, from the WWLLN network, classified into monthly intervals: July 1–31, 2014, August 1–31, 2014, and September 1–30, 2014. Period of time, total number of flashes, and monthly percentage with respect to the total is indicated in the upper-right corner of each panel. The 500-, 1,000-, and 2,000-m contours of terrain elevation are shown in white lines [Colour figure can be viewed at wileyonlinelibrary.com]

6-hr period (UTC)

	1800–2359	0000–0559	0600–1159	1200–1759
24 hr period	2,969	24,234	21,759	15,274
Rank Jul	29	1	2	1
Rank Jul-Sep	77	5	6	7
Jul average	6,504	8,990	6,269	3,842
Aug average	6,282	11,130	9,774	6,939
Sep average	3,963	6,787	7,101	4,703

TABLE 3 Number of lightning flashes from the WWLLN network in the area shown in Figure 10, for the 92-day period from July 1 to September 30, 2014

Note: The 24-hr period is from 1800 UTC 23 July through 1759 UTC 24 July. Ranks are for each 6-hr period with respect to July or July–September, 1 is for the most active case during the corresponding period. Monthly averages are computed from daily data and bold font represents values, in the 92-day period, above each average. Extreme records are indicated in bold.

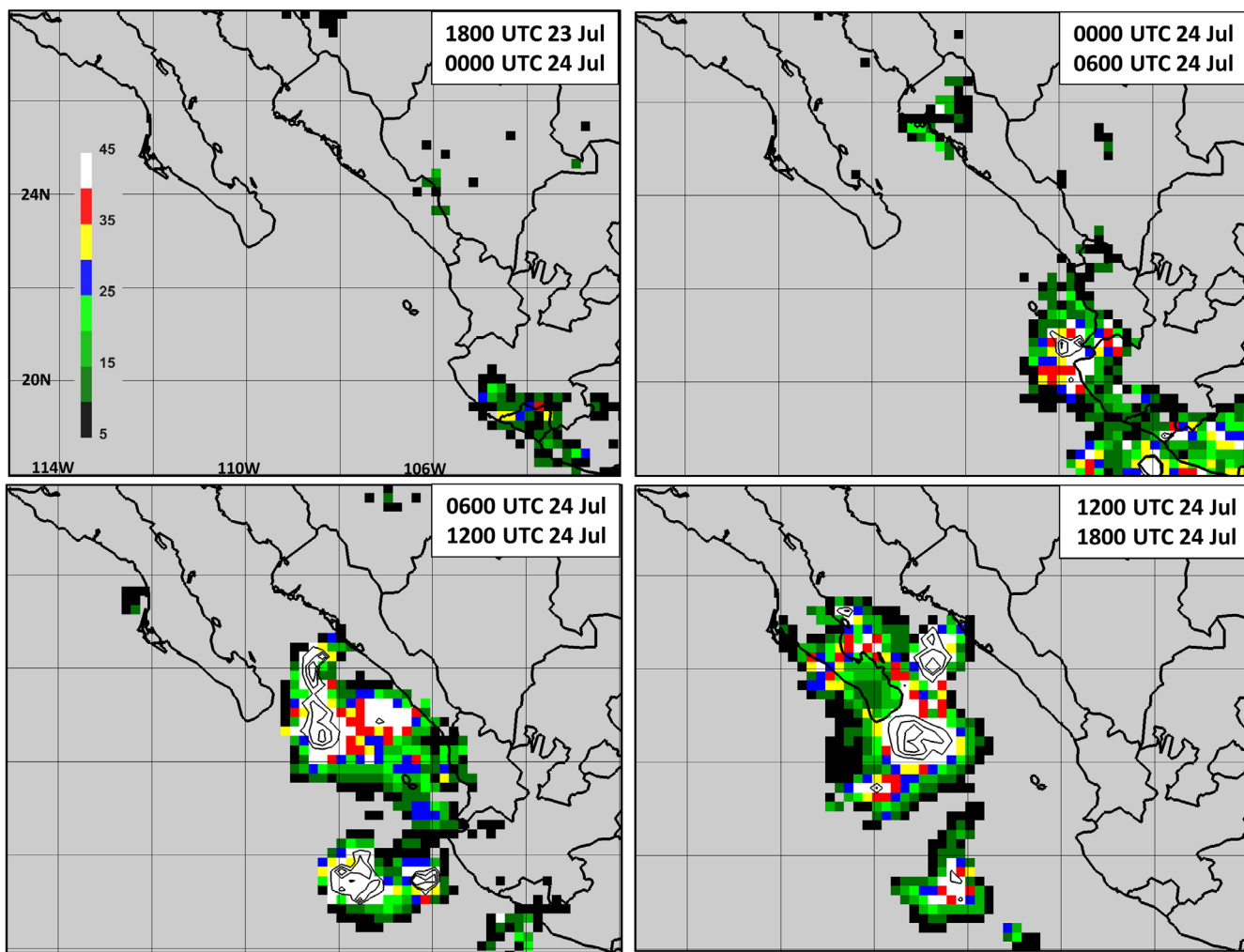


FIGURE 11 Accumulated rainfall (mm) estimated by the GPM satellite, at 6-hourly intervals, for the 24-hr period from 1800 UTC 23 July through 1800 UTC 24 July 2014. Black lines are contours for accumulations from 60 mm through 100 mm, at 20-mm intervals [Colour figure can be viewed at wileyonlinelibrary.com]

average, Los Cabos and the adjacent marine areas receive less than 50 mm per month during July over the 2009–2018 period (Figure 4). Therefore, at several locations, the MCS brought more precipitation in a single 12-hr period of July 24, 2014 than is typically received in the entire month.

4.2 | Surface conditions

At Islas Marías on the east side of the gulf entrance, from 1500 UTC 23 July to 0600 UTC 24 July (Figure 12a), the water vapour mixing ratio was nearly 20 g kg^{-1} , and similar conditions are observed at coastal stations in Jalisco and Nayarit (not shown). There was gradual backing of the surface wind, from north-northwesterly around 1230–2200 UTC 23 July, to southwesterly and then southerly at 0600 UTC 24 July, just before the MCS passage.

Maximum intensity with 14 m s^{-1} sustained speed (22.0 m s^{-1} peak gust) occurred at 0700 UTC; however, limited rainfall (1.8 mm) was collected, suggesting that the station was at the outer edge of the MCS. Drier conditions occurred after the MCS passage, with mixing ratio reduced to $15\text{--}18 \text{ g kg}^{-1}$; however, the data collection ended at 1845 UTC. Note that during the analysis period, the MCS brought a modest change to the local weather conditions.

On the west side of the gulf entrance, the MCS produced 17.8 mm of rainfall in Cabo San Lucas from 1340 to 1630 UTC 24 July (Figure 12b). This amount is 8% of the site's annual average, and is 26% larger than the July average, based on the 1937–2018 climatology. Before the MCS arrival, the air temperature was relatively constant ($25\text{--}27^\circ\text{C}$), as was the mixing ratio (20 g kg^{-1}). Then, strong southeasterly winds, with speeds up to 26.2 m s^{-1} (34.7 m s^{-1} peak gust), were detected at 1350 UTC. That

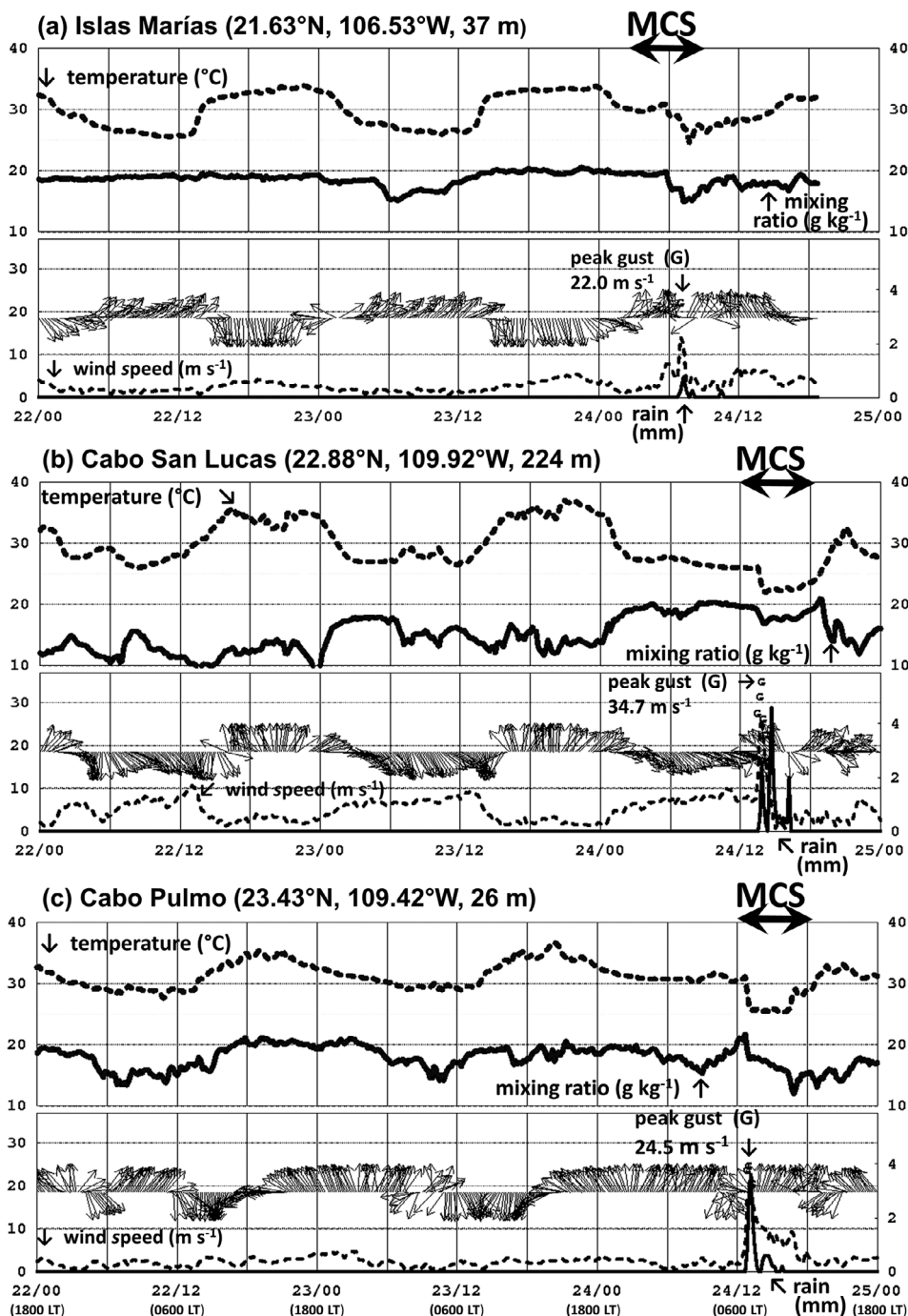


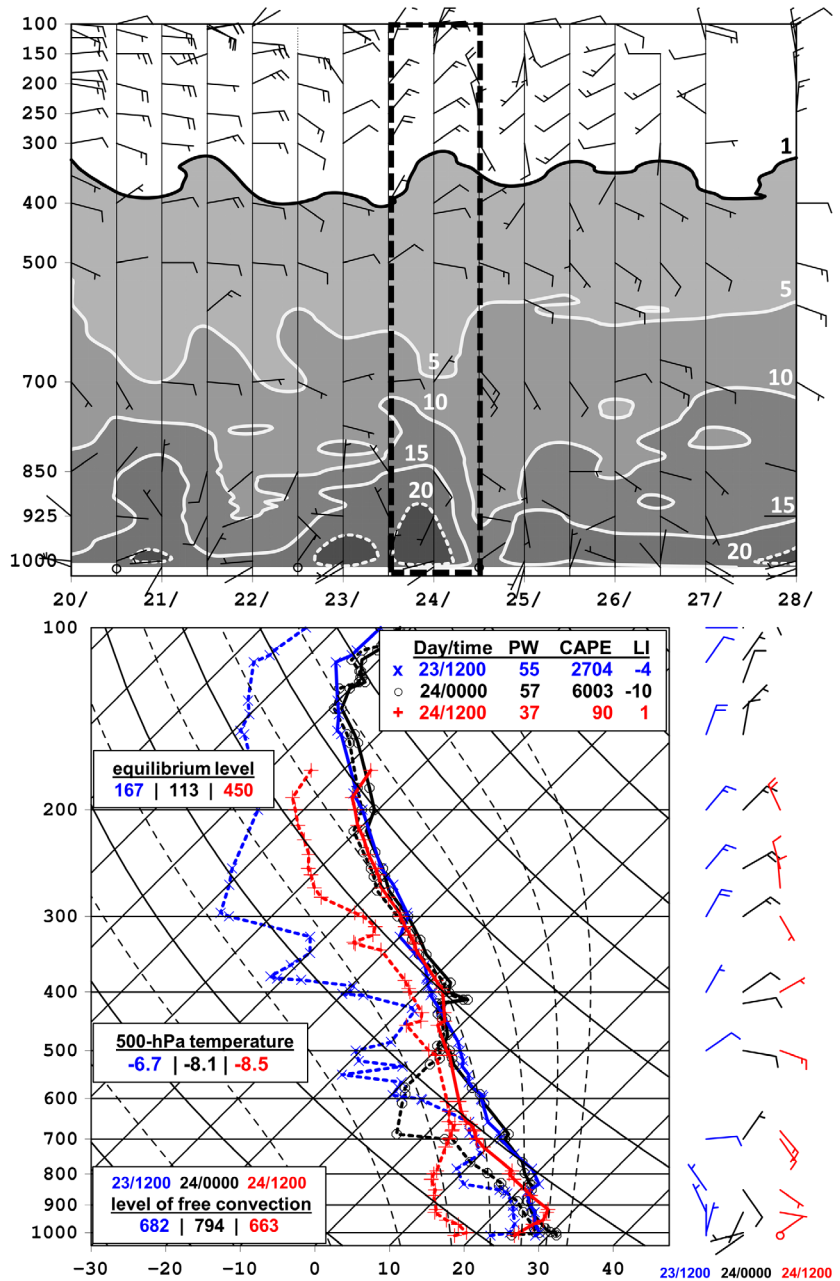
FIGURE 12 Surface observations from (a) Islas Marías, Nayarit, (b) Cabo San Lucas, Baja California Sur, and (c) Cabo Pulmo, Baja California Sur, for the period 0000 UTC 22 July–0000 UTC 25 July 2014. Position and station elevation above sea level are in parenthesis. Top panels show air temperature (dashed line) and mixing ratio (solid line) while bottom panels show peak gust (letter G), rainfall (solid line), sustained wind speed (dashed line), and wind direction (arrow). Temporal resolution is 15 min for (a), and 10 min for (b) and (c). The thick line with two arrows is the approximate passage, of the MCS, derived from the GOES satellite

contrasts sharply with typical northwesterly winds, during the late night and morning (0300–1500 UTC or 2100–0900 LT), in July 2014. On 24 July, for at least 30 min, wind speeds remained above 20 m s^{-1} , peak gusts exceeded 25 m s^{-1} , the temperature fell 4°C , and the air became drier. These conditions are similar to the assessed changes from gust fronts as documented by Charba (1974) in central Oklahoma and by Smith and Gall (1989) from MCSs in the northern SMO.

Local newspapers reported damage to trees and buildings, and there were delays at Los Cabos international

airport associated with reports of a thunderstorm, reduced visibility, rainfall, and gust up to 21 m s^{-1} between 1300 and 1700 UTC 24 July. Ground-level conditions changed rapidly in association with the MCS arrival; evaporatively driven downdrafts and an intense gust front at the surface were the likely cause of the property damage. At 1300 UTC, a station on the coast (Cabo Pulmo; Figures 2 and 12c), 80 km northeast of Cabo San Lucas, recorded maximum sustained wind (peak gust) up to 18.4 m s^{-1} (24.5 m s^{-1}) along with temperature and mixing ratio adjustments. Another station located at

FIGURE 13 Time series of horizontal winds from Manzanillo, Colima, from 20 to 28 July, 2014 soundings (top). The vertical axis is pressure (1000–100 hPa) and date labels are at 0000 UTC. Mixing ratio above 1 g kg^{-1} is shaded. Full wind barb is 5.0 m s^{-1} and half barb is 2.5 m s^{-1} . The dashed box outlines the relevant period in this study. Skew-T log p diagram from three consecutive Manzanillo soundings (bottom). Solid (dashed) lines are air (dew point) temperature in $^{\circ}\text{C}$. Calculated values of precipitable water (PW, mm), CAPE (J kg^{-1}), 500-hPa lifted index (LI, $^{\circ}\text{C}$), 500-hPa air temperature ($^{\circ}\text{C}$), level of free convection (hPa) and equilibrium level (hPa) are given [Colour figure can be viewed at wileyonlinelibrary.com]



1,950 m recorded sustained wind up to 16.4 m s^{-1} (24.0 m s^{-1} gust) at 1450 UTC and precipitation between 1500 and 1800 UTC; see Figure 2 (feature 10) for the station position. Therefore, the gust front affected the south-eastern coast of Los Cabos and the higher-elevation terrain that is consistent with WWLLN chronology (Figure 8).

4.3 | Upper-air features

Figure 13 shows a time series of the Manzanillo soundings. During the period 21–23 July, easterly flow in the 700–500 hPa layer prevailed before the MCS formation.

Considerable moisture was also present between 925 hPa and the surface, with a $10\text{--}20 \text{ g kg}^{-1}$ mixing ratio. At 0000 UTC 24 July, when convective clusters developed over coastal Colima and Jalisco (Figure 7), the 1,000-hPa mixing ratio reached a peak of 25 g kg^{-1} ; the corresponding thermodynamic diagram (Figure 13) depicts a more humid profile from the surface up to the 700-hPa level than the profile 12 hr earlier. Note a cyclonic wind shift, in the 300–100 hPa layer, from north-westerly to southwesterly during the 12 hr ending at 0000 UTC 25 July; this feature is associated with the passage of an upper-level trough. Also, there is clockwise turning of the winds in the 800–400 hPa layer, from northeasterlies at 1200 UTC 23 July to southeasterlies at 1200 UTC

Day (0000 UTC)									
	20	21	22	23	24	25	26	27	28
CAPE	1,611	3,536	1,413	5,331	6,003	2,564	1,567	2,019	4,103
LI	-2	-3	0	-8	-10	-1	0	-1	-4
PW	61	52	38	51	57	48	44	48	55
CIN	-177	-98	-262	-7	-1	-1	-115	-1	-2
T500	-3.9	-5.7	-6.3	-5.9	-8.1	-6.9	-5.5	-5.7	-5.3

Note: Only 0000 UTC releases are used. Values are for mixed-layer convective available potential energy (CAPE, J kg^{-1}), LI (LI, $^{\circ}\text{C}$), Precipitable water (PW, mm), mixed-layer convective inhibition (CIN, J kg^{-1}), and air temperature at 500 hPa (T500). For each parameter, extreme values are set in bold.

24 July associated with a tropical wave. Similar wind shifts are seen at other SMN stations, and more information, from gridded analyses, is provided in Section 4.4.

Table 4 provides mixed-layer CAPE, LI, PW, mixed-layer CIN, and 500-hPa air temperature from eight consecutive days starting on 20 July derived from the Manzanillo soundings. Most parameters reached extreme values on 24 July, including a CIN minimum (1 J kg^{-1}) after the MCS had already initiated. The LI reached -10°C , which is colder than values in the range of -5 to -8°C reported for western Mexico MCSs (Maddox and Howard, 1988) and also much colder than -3 to -4°C from MCSs in the northern SMO (Smith and Gall, 1989). In our case, the LI minimum is partially due to cold 500-hPa temperature, between -8 and -9°C , compared with -5.6°C , which was the average in July 2014. At 0000 UTC 24 July, the level of free convection reached a 794 hPa minimum, or 2.1 km, which suggests cell initiation within the moist boundary layer, typical of tropical MCSs (Barnes and Sieckman, 1984) and the equilibrium level was 113 hPa, roughly 16 km. Note that the temperature and dew-point profiles highlight a relatively dry, stable boundary layer behind the MCS, resembling the environment behind convective lines over the ocean (e.g., Zipser, 1977).

A similar analysis was performed on the upper-air data from Mazatlán, Sinaloa (23.20°N , 106.42°W , 4 m). But, results are not shown here because of the limited number of levels at 1200 UTC 23 July and 0000 UTC 24 July, along with missing soundings afterward, when the MCS moved across the gulf entrance. Despite the gap, the available dataset resulted in large CAPE (up to $4,912 \text{ J kg}^{-1}$), cold LI (-9 to -10°C), and enhanced PW (57 to 62 mm). These values are comparable to Manzanillo parameters in Table 4 and Figure 13; therefore, prior to the MCS approach, the gulf entrance was characterized by a favourable environment to support deep convection. Also, the air temperature at 500 hPa was -6.3°C

at 0000 UTC 24 July and -8.7°C at 1200 UTC 25 July, which is lower than the July 2014 average (-5.7°C) at this station.

4.4 | Large-scale flow

Tropical waves and inverted upper-level troughs are synoptic-scale features present during the evolution of the warm season in North America (e.g., Douglas and Englehart, 2007). Seastrand *et al.* (2015) state that the climatological position of the monsoon anticyclone over the southwestern United States allows persistent southeasterly flow and enhanced moisture, from low to middle levels, into the monsoon region. This moisture transport favours episodes with convective activity and heavy rainfall across northwestern Mexico. Such a setting resembles components we found to be present while the extraordinary MCS from July 24, 2014 developed but, in our case, the affected area is limited to the Gulf of California entrance and part of Baja California.

Figure 14 shows the spatial distribution of geopotential heights and anomalies at four pressure levels (200, 500, 700, and 850 hPa). Note that north of the area of the MCS detection, over northern Mexico and the southwestern United States, there is a mid- to upper-level anticyclone present with anomalies 20–100 m above the 2009–2018 average. This anticyclone resembles the classic pattern in thunderstorms over the northern SMO (e.g., Smith and Gall, 1989) and central Arizona (McCollum *et al.*, 1995). In addition, at 200 hPa, there is a cyclonic circulation in central Mexico with a well-defined area of lower than average (20–40 m) heights. Inspection of the analyses from previous days reveals that this circulation moved from the northern Gulf of Mexico along the southeastern flank of the large anticyclone.

Over the Gulf of California entrance, ERA5 data show flow with a westerly component at the surface along with

TABLE 4 Thermodynamic parameters from Manzanillo, Colima, upper-air soundings for the period July 20–28, 2014

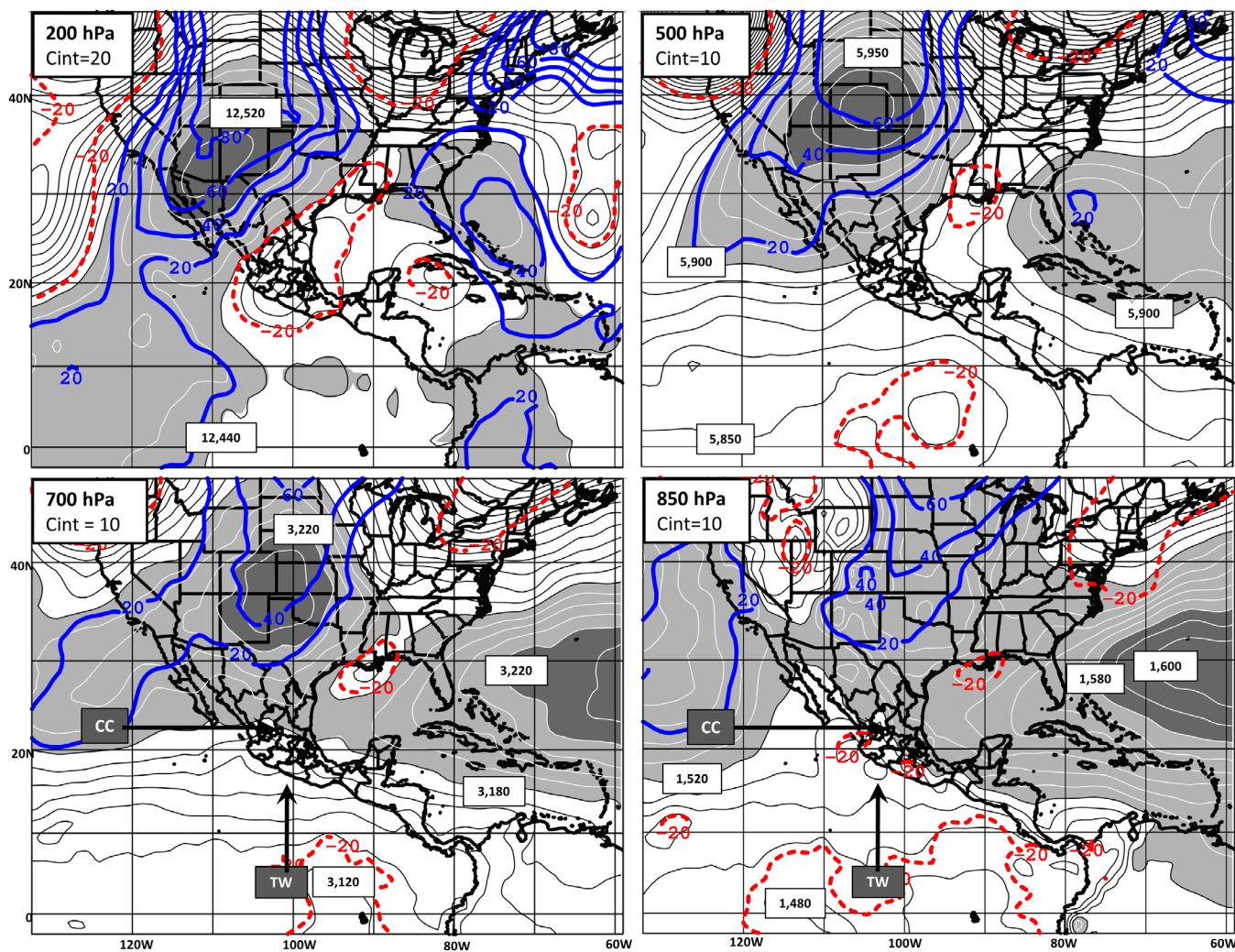


FIGURE 14 Geopotential height (thin lines, m) and anomalies (thick lines, m) at 0000 UTC 24 July 2014 from the ERA5 analyses at the 200-, 500-, 700-, and 850-hPa levels. Selected height contours are both labelled and shaded; Cint gives the corresponding height contour interval in m. A cyclonic circulation (CC) and a tropical wave (TW) are labelled at 700 and 850 hPa. Anomalies from the July (1979–2018) climatology are shown for values above (solid) and below (dashed) the average, at 20-m intervals [Colour figure can be viewed at wileyonlinelibrary.com]

high PW (>45 mm) and CAPE ($>5,000 \text{ J kg}^{-1}$). These values are consistent with the Manzanillo and Mazatlán upper-air observations discussed above; however, they are larger than those from the MCSs associated with other dates in Table 1. Additionally, there are further differences between the composite from the most unstable days (Figure 6) and the fields associated the extraordinary event (Figure 14). Among the relevant differences, on 24 July, there is:

- A stronger 200-, 500-, and 700-hPa anticyclone along with a northward displacement of the circulation centre over the area bounded by 30°N , 45°N , 90°W , and 120°W , which implies westward steering flow for MCS motion over the gulf entrance.
- At 700 hPa, a better-defined trough associated with the tropical wave off the southern coast of Mexico (within

$100\text{--}105^\circ\text{W}$) and, at 850 hPa, a small-scale, closed circulation near the coast of Colima, Jalisco, and Nayarit.

- An inverted trough along the southeastern edge of the 200-hPa anticyclone, over central Mexico (15°N , 25°N , 95°W , 105°W). Inverted troughs associated with most of the other days, listed in Table 1, are located farther west of 110°W over the Pacific Ocean.

5 | SUMMARY AND CONCLUSION

We used cloud-top temperature from geostationary satellites to investigate general characteristics (location, time, and intensity) of organized convection over northwestern Mexico, the Pacific Ocean, and the Baja California Peninsula. Our study extends previous climatologies by

covering the period 2009–2018 and focusing on July, in the early part of the warm season, when there is less influence of tropical cyclones from the eastern Pacific.

Our results indicate that besides the convective patterns over the SMO, there is a distinct area of persistent deep convection and heavy precipitation over the eastern edge of the Gulf of California entrance, offshore from Nayarit. According to remotely sensed (GPM) estimates from the 10-year climatology, in August and September, the corresponding rainfall accumulations are 1–2 times higher than those from the core of the North American Monsoon in Sinaloa and Sonora. This maximum is due, in part, to the frequent occurrence of MCSs that are active during more than 12 hr and remain almost stationary. Nevertheless, a few gulf entrance MCSs propagate northwestward to eventually reach Los Cabos in the southern tip of the peninsula.

In addition to the updated climatology, we analyse a unique extreme event observed on July 23 and 24, 2014 whose impacts serve to highlight the potential risk associated with long-lived MCSs. The system initiated over mainland Mexico, moved offshore into the gulf entrance, and more than 12 hr later, reached Los Cabos. Sustained winds in the range of tropical-storm strength resulted in property damage but, fortunately, no fatalities. To better understand this MCS, we examined upper-air observations from 1976–2018 and identified the top-10 days with large CAPE in the gulf entrance. The environment was more unstable, since 2012, and more favourable for the development of organized convection.

Our findings should guide weather forecasters and emergency managers whose responsibility is to protect the population and infrastructure along the coast of mainland Mexico and in Los Cabos, Baja California Sur. Based on our results, we suggest that future studies on MCSs that propagate across the gulf entrance may wish to explore: (a) the identification of physical mechanisms and processes that lead to fast (versus slow) translation motion; (b) the role of the SMO topography in the low-level (upslope and downslope) flow of moist air; and (c) the influence of mesoscale circulations that may be critical in the development of intense, long-lived MCSs. The states of Nayarit and Baja California Sur have tourism-based, coastal communities that are experiencing the fastest growth rates in Mexico, and two of these communities are in Los Cabos (SUN, 2018). These facts imply that some of the research efforts must be oriented to determine possible tracks, structure, and impacts from MCSs coming from the gulf entrance and, for the next few decades, estimates of the potential changes that these MCSs are likely to follow.

ACKNOWLEDGEMENTS

Surface and radar observations are from SMN; additional surface observations were provided by Secretaría de Marina. The GOES imagery is available from the Unidata Program Center at the University Corporation for Atmospheric Research and the Space Science and Engineering Center of the University of Wisconsin. The GPM dataset was courtesy of NASA's Goddard Space Flight Center and the Giovanni online data system (<https://giovanni.gsfc.nasa.gov/giovanni>). *The authors are grateful to the WWLLN (<http://wwlln.net>) for providing the lightning dataset.* This study was funded by CICESE (grant 691-103) and the PAPIIT program at UNAM (grants IA104416 and IA101418), with partial support from the visiting scientist program from UNAM-DGAPA and the Fulbright Scholar program at the U.S. Department of State. The authors wish to thank the reviewers for their comments and suggestions.

ORCID

Luis M. Farfán  <https://orcid.org/0000-0002-9719-1645>

Bradford S. Barrett  <https://orcid.org/0000-0002-5575-9052>

G. B. Raga  <https://orcid.org/0000-0002-4295-4991>

Julián J. Delgado  <https://orcid.org/0000-0002-9904-0576>

REFERENCES

- Adang, T.C. and Gall, R.L. (1989) Structure and dynamics of the Arizona monsoon boundary. *Monthly Weather Review*, 117(7), 1423–1437. [https://doi.org/10.1175/1520-0493\(1989\)117<1423:SADOTA>2.0.CO;2](https://doi.org/10.1175/1520-0493(1989)117<1423:SADOTA>2.0.CO;2).
- Adams, D.K. and Comrie, A.C. (1997) The North American monsoon. *Bulletin of the American Meteorological Society*, 78(10), 2197–2213. <https://doi.org/10.1175/1520-0477%281997%29078%3C2197%3ATNAM%3E2.0.CO%3B2>.
- Albrecht, R.I., Goodman, S.J., Buechler, D.E., Blakeslee, R.J. and Christian, H.J. (2016) Where are the lightning hotspots on earth? *Bulletin of the American Meteorological Society*, 97(11), 2051–2068. <https://doi.org/10.1175/BAMS-D-14-00193.1>.
- Barrett, B.S., Farfán, L.M., Raga, G.B. and Hernández, D.H. (2017) The unusual early morning tornado in Ciudad Acuña, Coahuila, Mexico on 25 May 2015. *Monthly Weather Review*, 145(6), 2049–2069. <https://doi.org/10.1175/MWR-D-16-0252.1>.
- Barnes, G.M. and Sieckman, K. (1984) The environment of fast-and slow-moving tropical mesoscale convective cloud lines. *Monthly Weather Review*, 112(9), 1782–1794. [https://doi.org/10.1175/1520-0493\(1984\)112%3C1782:TEOFAS%3E2.0.CO;2](https://doi.org/10.1175/1520-0493(1984)112%3C1782:TEOFAS%3E2.0.CO;2).
- Bluestein, H.B. and Jain, M.H. (1985) Formation of mesoscale lines of precipitation: severe squall lines in Oklahoma during the spring. *Journal of the Atmospheric Sciences*, 42(16), 1711–1732. [https://doi.org/10.1175/1520-0469\(1985\)042%3C1711:FOMLOP%3E2.0.CO;2](https://doi.org/10.1175/1520-0469(1985)042%3C1711:FOMLOP%3E2.0.CO;2).
- Brito-Castillo, L., Vivoni, E.R., Gochis, D.J., Filonov, A., Tereshchenko, I. and Monzón, C. (2010) An anomaly in the occurrence of the month of maximum precipitation distribution

- in Northwest Mexico. *Journal of Arid Environments*, 74(5), 531–539. <https://doi.org/10.1016/j.jaridenv.2009.10.014>.
- Brooks, H.E., Doswell, C.A., III, Zhang, X., Chernokulsky, A., Tochimoto, E., Hanstrum, B., de Lima Nascimento, E., Sills, D. M.L., Antonescu, B. and Barrett, B.S. (2019) A century of progress in severe convective storm research and forecasting. *Meteorological Monographs*, 59, 18.1–18.41. <https://doi.org/10.1175/AMSMONOGRAPHSD-18-0026.1>.
- Charba, J. (1974) Application of gravity current model to analysis of squall-line gust front. *Monthly Weather Review*, 102(2), 140–156. [https://doi.org/10.1175/1520-0493\(1974\)102<0140:AOGCMT>2.0.CO;2](https://doi.org/10.1175/1520-0493(1974)102<0140:AOGCMT>2.0.CO;2).
- Cortez Vazquez, M. (1999) Marcha anual de la actividad convectiva en Mexico. *Atmósfera*, 12(2), 101–110 Available at: <https://www.revistascca.unam.mx/atm/index.php/atm/article/view/28132>.
- Deierling, W. and Petersen, W.A. (2008) Total lightning activity as an indicator of updraft characteristics. *Journal of Geophysical Research - Atmospheres*, 113, D16210. <https://doi.org/10.1029/2007JD009598>.
- Dotzek, N., Rabin, R.M., Carey, L.D., MacGorman, D.R., McCormick, T.L., Demetriades, N.W., Murphy, M.J. and Holle, R.L. (2005) Lightning activity related to satellite and radar observations of a mesoscale convective system over Texas on 7–8 April 2002. *Atmospheric Research*, 76(1–4), 127–166. <https://doi.org/10.1016/j.atmosres.2004.11.020>.
- Douglas, M.W., Maddox, R.A. and Howard, K. (1993) The Mexican monsoon. *Journal of Climate*, 6(8), 1665–1677. [https://doi.org/10.1175/1520-0442\(1993\)006%3C1665:TMM%3E2.0.CO;2](https://doi.org/10.1175/1520-0442(1993)006%3C1665:TMM%3E2.0.CO;2).
- Douglas, A.V. and Englehart, P.J. (2007) A climatological perspective of transient synoptic features during NAME 2004. *Journal of Climate*, 20, 1947–1954. <https://doi.org/10.1175/JCLI4095.1>.
- Durre, I., Vose, R.S. and Wuertz, D.B. (2006) Overview of the integrated global radiosonde archive. *Journal of Climate*, 37(3), 1753–1770. <https://doi.org/10.1175/JTECH-D-17-0223.1>.
- Farfán, L.M. and Zehnder, J.A. (1994) Moving and stationary mesoscale convective systems over Northwest Mexico during the Southwest Area Monsoon Project. *Weather and Forecasting*, 9(4), 630–639. [https://doi.org/10.1175/1520-0434\(1994\)009<0630:MASMCS>2.0.CO;2](https://doi.org/10.1175/1520-0434(1994)009<0630:MASMCS>2.0.CO;2).
- Farfán, L.M. (2005) Development of convective systems over Baja California during tropical cyclone Linda (2003). *Weather and Forecasting*, 20(5), 801–811. <https://doi.org/10.1175/WAF879.1>.
- García, E. and Trejo, R.I. (1990) Causas de la precipitación en Nayarit. *Memoria del XII Congreso Nacional de Geografía*. Tepic, Mexico: Sociedad Mexicana de Geografía y Estadística e Instituto Nacional de Estadística, pp. 234–243.
- García, E. and Trejo, R.I. (1994) La presencia del monzón en el noroeste de México. *Investigaciones Geográficas*, 1(28), 33–64. <https://doi.org/10.14350/rig.59024>.
- García-Oliva, F., Ezcurra, E. and Galicia, L. (1991) Pattern of rainfall distribution in the Central Pacific Coast of Mexico. *Geografiska Annaler, Series A—Physical Geography*, 73(3/4), 179–186. <https://doi.org/10.1080/04353676.1991.11880343>.
- Garreaud, R. and Wallace, J.M. (1997) The diurnal march of convective cloudiness over the Americas. *Monthly Weather Review*, 125(12), 3157–3171. [https://doi.org/10.1175/1520-0493\(1997\)125<3157:TDMOCC>2.0.CO;2](https://doi.org/10.1175/1520-0493(1997)125<3157:TDMOCC>2.0.CO;2).
- Gebremichael, M., Vivoni, E.R., Watts, C.J. and Rodríguez, J.C. (2007) Submesoscale spatiotemporal variability of North American monsoon rainfall over complex terrain. *Journal of Climate*, 20(9), 1751–1773. <https://doi.org/10.1175/JCLI4093.1>.
- Gochis, D.J., Nesbitt, S.W., Yu, W. and Williams, S.F. (2009) Comparison of gauge-corrected versus non-gauge corrected satellite-based quantitative precipitation estimates during the 2004 NAME enhanced observing period. *Atmosfera*, 22(1), 119–149 Available at: <https://www.revistascca.unam.mx/atm/index.php/atm/article/view/8620>.
- Goodman, S.J., Schmit, T.J., Daniels, W., Denig, W. and Metcalf, K. (2017) GOES: past, present, and future. In: Liang, S. (Ed.) *Comprehensive Remote Sensing*. Amsterdam: Elsevier, pp. 119–149. <https://doi.org/10.1016/B978-0-12-409548-9.10315-X>.
- González-Elizondo, M.S., González-Elizondo, M., Tena-Flores, J.A., Ruacho-González, L. and López-Enríquez, I.L. (2012) Vegetación de la Sierra Madre Occidental, México: una síntesis. *Acta Botánica Mexicana*, (100), 351–403 Available at: http://www.scielo.org.mx/scielo.php?script=sci_arttext&pid=S0187-71512012000300012.
- Hersbach, H., Bell, B., Berrisford, P., Hirahara, S., Horányi, A., Muñoz-Sabater, J., Nicolas, J., Peubey, C., Radu, R., Schepers, D., Simmons, A., Soci, C., Abdalla, S., Abellán, X., Balsamo, G., Bechtold, P., Biavati, G., Bidlot, J., Bonavita, M., Chiara, G., Dahlgren, P., Dee, D., Diamantakis, M., Dragani, R., Flemming, J., Forbes, R., Fuentes, M., Geer, A., Haimberger, L., Healy, S., Hogan, R.J., Hólm, E., Janisková, M., Keeley, S., Laloyaux, P., Lopez, P., Lupu, C., Radnoti, G., Rosnay, P., Rozum, I., Vamborg, F., Villaume, S. and Thépaut, J.N. (2020) The ERA5 global reanalysis. *Quarterly Journal of the Royal Meteorological Society*, 1–51. <https://doi.org/10.1002/qj.3803>.
- Higgins, W. and Gochis, D. (2007) Synthesis of results from the North American monsoon experiment (NAME) process study. *Journal of Climate*, 20(9), 1601–1607. <https://doi.org/10.1175/JCLI4081.1>.
- Holle, R.L. and Murphy, M.J. (2015) Lightning in the North American monsoon: an exploratory climatology. *Monthly Weather Review*, 143(5), 1970–1977. <https://doi.org/10.1175/MWR-D-14-00363.1>.
- Houze, R.A., Jr. (2004) Mesoscale convective systems. *Reviews of Geophysics*, 42, RG4003. <https://doi.org/10.1029/2004RG000150>.
- Howard, K.W. and Maddox, R.A. (1988a) Mexican mesoscale convective systems—a satellite perspective. In: *Proceedings of Third International American and Mexican Congress of Meteorology, Mexican Meteorological Organization*. Mexico City: Mexican Meteorological Organization, pp. 404–408.
- Howard, K.W. and Maddox, R.A. (1988b) A satellite-based climatology of warm season thunderstorms over Mexico. In: *Proceedings of Third International American and Mexican Congress of Meteorology, Mexican Meteorological Organization*. Mexico City: Mexican Meteorological Organization, pp. 414–417.
- Huffman, G.J., Bolvin, D.T., Braithwaite, D., Hsu, K., Joyce, R., Kidd, C., Nelkin, E.J., Sorooshian, S., Tan, T., Xie, P. (2019). NASA Global Precipitation Measurement (GPM) Integrated Multi-satellite Retrievals for GPM (IMERG). Algorithm Theoretical Basis Document (ATBD) Version 06. Available at:

- https://pmm.nasa.gov/sites/default/files/document_files/IMERG_ATBD_V06.pdf.
- Laing, A.G. and Fritsch, J.M. (1993a) Mesoscale convective complexes over the Indian monsoon region. *Journal of Climate*, 6(5), 911–919. [https://doi.org/10.1175/1520-0442\(1993\)006<0911:MCCOTI>2.0.CO;2](https://doi.org/10.1175/1520-0442(1993)006<0911:MCCOTI>2.0.CO;2).
- Laing, A.G. and Fritsch, J.M. (1993b) Mesoscale convective complexes in Africa. *Monthly Weather Review*, 121(8), 2254–2263. [https://doi.org/10.1175/1520-0493\(1993\)121<2254:MCCIA>2.0.CO;2](https://doi.org/10.1175/1520-0493(1993)121<2254:MCCIA>2.0.CO;2).
- Laing, A.G. and Fritsch, J.M. (1997) The global population of mesoscale convective complexes. *Quarterly Journal of the Royal Meteorological Society*, 123, 389–405. <https://doi.org/10.1002/qj.49712353807>.
- Laing, A.G. and Fritsch, J.M. (2000) The large-scale environments of the global populations of mesoscale convective complexes. *Monthly Weather Review*, 128(8), 2756–2776. [https://doi.org/10.1175/1520-0493\(2000\)128<2756:TLSEOT>2.0.CO;2](https://doi.org/10.1175/1520-0493(2000)128<2756:TLSEOT>2.0.CO;2).
- Laing, A. (2015) Mesoscale convective systems. In: North, G.R., Pyle, J. and Zhang, F. (Eds.) *Encyclopedia of Atmospheric Sciences*, 2nd edition. Amsterdam, The Netherlands: Elsevier, pp. 339–354. <https://doi.org/10.1016/B978-0-12-382225-3.00216-4>.
- Lang, T., Ahijevych, D., Nesbitt, S., Carbone, R.E., Rutledge, S.A. and Cifelli, R. (2007) Radar-observed characteristics of precipitating systems during NAME 2004. *Journal of Climate*, 20(9), 1713–1733. <https://doi.org/10.1175/JCLI4082.1>.
- Lang, T., Pédeboy, S., Rison, W., Cerveny, R.S., Montanyà, J., Chauzy, S., MacGorman, D.R., Holle, R.L., Ávila, E.E., Zhang, Y., Carbin, G., Mansell, E.R., Kuleshov, Y., Peterson, T. C., Brunet, M., Driouech, F. and Krahenbuhl, D.S. (2017) WMO world record lightning extremes: longest reported flash distance and longest reported flash duration. *Bulletin of the American Meteorological Society*, 98(6), 1153–1168. <https://doi.org/10.1175/BAMS-D-16-0061.1>.
- Latorre, C. and Penilla, L. (1988) Influence of cyclones in the precipitation of Baja California Sur. *Atmósfera*, 1(2), 99–112 Available at: <https://www.revistascca.unam.mx/atm/index.php/atm/article/view/8268>.
- LeMone, M.A., Zipser, E.J. and Trier, S.B. (1998) The role of environmental shear and thermodynamic conditions in determining the structure and evolution of mesoscale convective systems during TOGA COARE. *Journal of the Atmospheric Sciences*, 55(23), 3493–3518. [https://doi.org/10.1175/1520-0469\(1998\)055<3493:TROESA>2.0.CO;2](https://doi.org/10.1175/1520-0469(1998)055<3493:TROESA>2.0.CO;2).
- Liebmann, B., Bladé, I., Bond, N.A., Gochis, D., Allured, D. and Bates, G.T. (2008) Characteristics of north American summertime rainfall with emphasis on the monsoon. *Journal of Climate*, 21(6), 1277–1294. <https://doi.org/10.1175/2007JCLI1762.1>.
- Machado, L.A.T., Rossow, W.B., Guedes, R.L. and Walker, A.W. (1998) Life cycle variations of mesoscale convective systems over the Americas. *Monthly Weather Review*, 126(8), 1630–1654. [https://doi.org/10.1175/1520-0493\(2004\)132%3C0714:TCSAE0%3E2.0.CO;2](https://doi.org/10.1175/1520-0493(2004)132%3C0714:TCSAE0%3E2.0.CO;2).
- Maddox, R.A. (1980) Mesoscale convective complexes. *Bulletin of the American Meteorological Society*, 61, 1374–1387. [https://doi.org/10.1175/1520-0477\(1980\)061<1374:MCC>2.0.CO;2](https://doi.org/10.1175/1520-0477(1980)061<1374:MCC>2.0.CO;2).
- Maddox, R.A. and Howard, K.W. (1988) Mexican mesoscale convective systems—Large scale environmental conditions. In: *Proceedings of the Third International American and Mexican Congress of Meteorology*. Mexico City, Mexico: Mexican Meteorological Organization, pp. 395–399.
- McCollum, D.M., Maddox, R.A. and Howard, K.W. (1995) Case study of a severe mesoscale convective system in Central Arizona. *Weather and Forecasting*, 10(3), 643–665. [https://doi.org/10.1175/1520-0434\(1995\)010<0643:CSOASM>2.0.CO;2](https://doi.org/10.1175/1520-0434(1995)010<0643:CSOASM>2.0.CO;2).
- Meitín, J.G., Howard, K.W. and Maddox, R.A. (1991) *Southwest Area Monsoon Project. Daily Operations Summary*. Norman, OK: National Severe Storms Laboratory.
- Mejia, J.F., Douglas, M.W. and Lamb, P.J. (2015) Observational investigation of relationships between moisture surges and mesoscale- to large-scale convection during the North American monsoon. *International Journal of Climatology*, 36, 2555–2569. <https://doi.org/10.1002/joc.4512>.
- Mosíño Alemán, P.A. and García, E. (1974) The climate of Mexico. *World survey of climatology*. In: Bryson, R.A. and Hare, F.K. (Eds.) *Climates of North America*. Amsterdam: Elsevier, pp. 345–404.
- Negri, A.J., Adler, R.F., Maddox, R.A., Howard, K.W. and Keehn, P. R. (1993) A regional rainfall climatology over Mexico and the Southwest United States derived from passive microwave and geosynchronous infrared data. *Journal of Climate*, 6(11), 2144–2161. [https://doi.org/10.1175/1520-0442\(1993\)006%3C2144:ARRCOM%3E2.0.CO;2](https://doi.org/10.1175/1520-0442(1993)006%3C2144:ARRCOM%3E2.0.CO;2).
- Negri, A.J., Adler, R.F., Nelkin, E.J. and Huffman, G.J. (1994) Regional rainfall climatologies derived from special sensor microwave imager (SSM/I) data. *Bulletin of the American Meteorological Society*, 75(7), 1165–1182. [https://doi.org/10.1175/1520-0477\(1994\)075%3C1165:RRCDFS%3E2.0.CO;2](https://doi.org/10.1175/1520-0477(1994)075%3C1165:RRCDFS%3E2.0.CO;2).
- Nesbitt, S.W., Gochis, D.J. and Lang, T.J. (2008) The diurnal cycle of clouds and precipitation along the Sierra Madre Occidental observed during NAME-2004: implications for warm season precipitation estimation in complex terrain. *Journal of Hydrometeorology*, 9(4), 728–743. <https://doi.org/10.1175/2008JHM939.1>.
- Palacios-Hernández, E., Brito-Castillo, L., Carrillo, L. and Tereshchenko, I. (2012) Interannual deviations of long-term data from observations and contrasting with reanalysis data from the oceanic station at Islas Marías, Nayarit, Mexico. *Atmósfera*, 25(4), 355–370 Available at: <https://www.revistascca.unam.mx/atm/index.php/atm/article/view/33695/30757>.
- Perdigón-Morales, J., Romero-Centeno, R., Pérez, P.O. and Barrett, B.S. (2018) The midsummer drought in Mexico: perspectives on duration and intensity from the CHIRPS precipitation database. *International Journal of Climatology*, 38(5), 2174–2186. <https://doi.org/10.1002/joc.5322>.
- Punkka, A. and Bister, M. (2015) Mesoscale convective systems and their synoptic-scale environment in Finland. *Weather and Forecasting*, 30(1), 182–196. <https://doi.org/10.1175/WAF-D-13-00146.1>.
- Raga, G.B., de la Parra, M.G. and Kucienska, B. (2014) Deaths by lightning in Mexico (1979–2011): threat or vulnerability? *Weather, Climate and Society*, 6(4), 434–444. <https://doi.org/10.1175/WCAS-D-13-00049.1>.

- Ray, A.J., Garfin, G.M., Wilder, M., Vásquez-León, M., Lenart, M. and Comrie, A.C. (2007) Applications of monsoon research: Opportunities to inform decision making and reduce regional vulnerability. *Journal of Climate*, 20(9), 1608–1627. <https://doi.org/10.1175/JCLI4098.1>.
- Reyes, S. and Cadet, D.L. (1988) The southwest branch of the North American Monsoon during summer 1979. . *Monthly Weather Review*, 116(5), 1175–1187. [https://doi.org/10.1175/1520-0493\(1988\)116<1175:TSBOTN>2.0.CO;2](https://doi.org/10.1175/1520-0493(1988)116<1175:TSBOTN>2.0.CO;2).
- Rowe, A.K., Rutledge, S.A. and Lang, T.J. (2011) Investigation of microphysical processes occurring in isolated convection during NAME. *Monthly Weather Review*, 139(2), 424–443. <https://doi.org/10.1175/2010MWR3494.1>.
- Rowe, A.K., Rutledge, S.A. and Lang, T.J. (2012) Investigation of microphysical processes occurring in organized convection during NAME. *Monthly Weather Review*, 140(7), 2168–2187. <https://doi.org/10.1175/MWR-D-11-00124.1>.
- Salio, P., Nicolini, M. and Zipser, E.J. (2007) Mesoscale convective systems over southeastern South America and their relationship with the south American low- level jet. *Monthly Weather Review*, 135(4), 1290–1309. <https://doi.org/10.1175/MWR3305.1>.
- Seastrand, S., Serra, Y., Castro, C. and Ritchie, E.A. (2015) The dominant synoptic-scale modes of North American monsoon precipitation. *International Journal of Climatology*, 35(8), 2019–2032. <https://doi.org/10.1002/joc.4104>.
- Smith, W.P. and Gall, R.L. (1989) Tropical squall lines of the Arizona monsoon. *Monthly Weather Review*, 117(7), 1553–1569. [https://doi.org/10.1175/1520-0493\(1989\)117<1553:TSLOTA>2.0.CO;2](https://doi.org/10.1175/1520-0493(1989)117<1553:TSLOTA>2.0.CO;2).
- Stensrud, D.J., Gall, R.L., Mullen, S.L. and Howard, K.W. (1995) Model climatology of the Mexican monsoon. *Journal of Climate*, 8(7), 1775–1794. [https://dx.doi.org/10.1175/1520-0442\(1995\)008%3C1775:MCOTMM%3E2.0.CO;2](https://dx.doi.org/10.1175/1520-0442(1995)008%3C1775:MCOTMM%3E2.0.CO;2).
- SUN. (2018) *Sistema Urbano Nacional*. Secretaría de Desarrollo Agrario, Territorial y Urbano; Consejo Nacional de Población: Available at https://www.gob.mx/cms/uploads/attachment/file/400771/SUN_2018.pdf
- Valdés-Manzanilla, A. (2015) Mesoscale convective systems in NW Mexico during the strong ENSO events of 1997-1999. *Atmósfera*, 28(2), 143–148. <https://doi.org/10.20937/ATM.2015.28.02.06>.
- Valdés-Manzanilla, A., Cortéz Vázquez, M. and Pastrana Francisco, J.J. (2005) Un estudio explorativo de los sistemas convectivos de mesoescala de México. *Investigaciones Geográficas*, 26, 26–42 Available at: <http://www.investigacionesgeograficas.unam.mx/index.php/rig/article/view/30094>.
- Vega-Camarena, J.P., Brito-Castillo, L. and Farfán, L.M. (2018) Contrasting rainfall behavior between the Pacific coast and the Mexican Altiplano. *Climate Research*, 76, 225–240. <https://doi.org/10.3354/cr01538>.
- Velasco, I. and Fritsch, J.M. (1987) Mesoscale convective complexes in the Americas. *Journal of Geophysical Research*, 92, 9591–9613. <https://doi.org/10.1029/JD092iD08p09591>.
- Vidal-Zepeda, R. and Hernández Cerdá, M.E. (1992) Algunas características de la precipitación en Nayarit, México. *Geografía y Desarrollo*, III(7), 9–18 Available at: http://internet.contenidos.inegi.org.mx/contenidos/productos/prod_serv/contenidos/espanol/bvinegi/productos/historicos/380/702825002235/702825002235_2.pdf.
- Virts, K.S. and Houze, R.A. (2016) Seasonal and intraseasonal variability of mesoscale convective systems over the south Asian monsoon region. *Journal of the Atmospheric Sciences*, 73(12), 4753–4774. <https://doi.org/10.1175/JAS-D-16-0022.1>.
- Wall, C.L., Zipser, E.J. and Liu, C. (2012) A regional climatology of monsoonal precipitation in the southwestern United States using TRMM. *Journal of Hydrometeorology*, 13(1), 310–323. <https://doi.org/10.1175/JHM-D-11-031.1>.
- Warner, T.T. (2004) *Desert Meteorology*. Cambridge, UK: Cambridge University Press. <https://doi.org/10.1017/CBO9780511535789>.
- Zipser, E.J. (1977) Mesoscale and convective-scale downdrafts as distinct components of squall-line circulation. *Monthly Weather Review*, 105(12), 1568–1589. [https://doi.org/10.1175/1520-0493\(1977\)105<1568:MACDAD>2.0.CO;2](https://doi.org/10.1175/1520-0493(1977)105<1568:MACDAD>2.0.CO;2).
- Zipser, E.J., Cecil, D.J., Liu, C., Nesbitt, S.W. and Yorty, D.P. (2006) Where are the most intense thunderstorms on earth? *Bulletin of the American Meteorological Society*, 87(8), 1057–1071. <https://doi.org/10.1175/BAMS-87-8-1057>.

How to cite this article: Farfán LM, Barrett BS, Raga GB, Delgado JJ. Characteristics of mesoscale convection over northwestern Mexico, the Gulf of California, and Baja California Peninsula. *Int J Climatol*. 2020;1–23. <https://doi.org/10.1002/joc.6752>